THE ASTROPHYSICAL JOURNAL, 346:735–755, 1989 November 15

THE PHOTOEVAPORATION OF INTERSTELLAR CLOUDS. I. RADIATION-DRIVEN IMPLOSION

FRANK BERTOLDI
Department of Physics, University of California, Berkeley
Received 1988 July 22; accepted 1989 May 15

ABSTRACT

In this and a subsequent paper we develop an approximate analytical solution for the evolution of an interstellar neutral cloud which is exposed to the ionizing radiation of a newly formed star. Generalizing the historic work by Oort, Spitzer, and Kahn, the structure of a steady photoevaporation gas flow off a spherical ionization front is derived even for cases where the ionization front cannot be considered thin and the downstream flow is not in ionization and thermal equilibrium. It is shown that under a wide range of conditions the ionization front is approximately D-critical and the ionized gas expands supersonically into the intercloud medium. We show that the ionization front typically drives a strong shock into the initial cloud. Clouds have different fates depending mainly on their initial column density and the ionization parameter at the location of the cloud. The clouds which are not instantly ionized will be compressed by an ionization-shock front which can focus the neutral gas into a compact globule. In an approximate way, it is shown how the ionization-shock front propagates into an initially spherical cloud. We treat the initial *radiation-driven implosion* under the assumption of axisymmetry, and derive both the cloud mass loss and the final velocity of the imploded globule. As a result of the rocket effect of the evaporating gas, the cloud gains a velocity of up to 5 km s^{-1} away from the ionizing source. It is shown that the focusing of gas onto the cloud symmetry axis causes an accretion shock through which the gas is compressed for a second time. We derive expressions for the pressure in the imploded cloud for both thermally and magnetically dominated clouds. The subsequent fate of the imploded cloud, the *equilibrium cometary stage*, will be discussed in Paper II. Our theory enables us to relate the observed photoevaporating clouds in H II regions to the region's initial cloud population. We point out the application of our model to the evolution of intergalactic Lyα clouds.

Subject headings: interstellar: matter — nebulae: H II regions — shock waves

I. INTRODUCTION

Interstellar H II regions are formed through the joint effects of the wind and ionizing radiation produced by one or more early-type stars. In the early phase of the H II region, a rapid R-type ionization front (I-front) propagates out to the Strömgren radius, while the strong wind of an O star will create a rapidly expanding ionized bubble. A neutral dense shell will form, driven by the thermal pressure of the ionized gas. Observations show that these neutral shells typically show very irregular structures and are often associated with small neutral clumps, some of which seem attached to large neutral regions, whereas others are isolated and fully embedded in the ionized gas.

The observed clumps are classified according to their appearance as elephant trunks, speck globules, bright rim clouds, or cometary globules (Leung 1985). Their shape is typically spherical or elongated and directed away from the main ionizing source. The bright rims are seen on the cloud's side facing the ionizing source (e.g., Pottasch 1956, 1958*a*, *b*). Typical sizes of these globules range from 0.05 to 1 pc, and densities range between 10^4 and 10^5 cm^{-3}. Where measurable, the globules seem to have high velocities of order 10 km s^{-1} away from the ionizing source.

Several explanations have been suggested for the origin of the neutral globules associated with H II regions. Some propose that the neutral condensations merely reflect density inhomogeneities in the initial medium (Dibai 1963; Reipurt 1983). Left behind by the rapidly expanding R-type I-front, they slowly evaporate while being accelerated away from the ionizing source by the rocket effect of their ejecta. Other models propose that instabilities in the neutral shells surrounding H II regions can form dense, elongated clumps. It has been suggested that their symmetrical, mostly elongated shape is due to the action of stellar winds, supernova explosions, or I-front–driven shocks. Kahn (1958) argued that elephant trunks cannot be formed through instabilities in planar ionization-shock fronts.

The photoevaporation and dynamics of the neutral clouds will have a significant effect on the evolution of the H II region as a whole. Most of the mass within visible ionized regions can probably be attributed to neutral dense clouds. The amount of mass transformed by photoevaporation from neutral globules to ionized gas, as well as the mass lost by globules escaping the H II region, will determine the structure of the region and affect the global dynamics of the interstellar medium. The photoevaporation of neutral globules will at the end determine the mean density of the H II region and provide the initial conditions for the expansion of a Type II supernova remnant (McKee, Van Buren, and Lazareff 1984; Shull *et al.* 1985).

The dense shells surrounding H II regions as well as the neutral globules have been cited as possible centers for star formation (Elmegreen and Lada 1977; Sandford, Whitaker, and Klein 1982). Some globules within the Gum Nebula seem to be associated with low-mass star formation, showing young stars or HH objects (Dibai 1960; Reipurth 1983). Understanding the evolution of neutral condensations is the key to answering the question whether star formation can be triggered by the dynamical effects of OB stars.

The fate of a cloud exposed to the ionizing radiation of an OB star was first extensively investigated by Oort and Spitzer (1955). In their approximate study they found that because of the rocket effect of the gas evaporated off the side of the cloud facing the star, clouds can be accelerated away from the ionizing star while losing part of their initial mass. They can gain velocities up to the mean escape velocity of the evaporating gas, which is estimated as 20 km s^{-1}. For their analysis, Oort and Spitzer ignored the dynamical effects of the photoevaporation on the cloud structure, which was assumed spherical and of constant radius during the cloud's evolution. When the ionizing star first turns on, the star's radiation will ionize and heat a surface layer, which will rapidly expand into the assumed vacuum surrounding the cloud. They suggested that a shock wave will advance into the neutral gas, but they did not attempt to investigate its effect on the later evolution of the cloud. Instead, a steady state was assumed to develop in which the ionized gas streams off the cloud surface at a constant velocity ($\sim$40 km s^{-1}) and constant temperature ($\sim 10^4$ K). The gas in this *insulating layer* (or *ionized boundary layer* [IBL] in Elmegreen 1976), which was estimated to have an effective thickness of half the cloud radius, recombines and thereby absorbs part of the incident ionizing photon flux. Only a fraction $1/f$ of the incident flux actually reaches the cloud surface to ionize the neutral cloud. In the cases they considered, $f \gg 1$.

Kahn (1969) investigated the flow of ionized gas off a neutral photoevaporating globule in more detail. Like Oort and Spitzer, he argued that most of the incident Lyman continuum photons are absorbed in the IBL, which has an effective thickness of about 0.2 times the cloud radius. In this case the I-front is thin compared with the width of the IBL and can be treated as a planar front, which has been investigated extensively (e.g., Kahn 1954; Axford 1961). A steady evaporation flow is possible if the gas can freely expand into the intercloud medium. Then the I-front propagates subsonically into the neutral cloud with the (strong D-type) velocity $u_{\rm IF}$, which is determined by the isothermal sound speed in the neutral gas, c_0, and the maximum sound speed in the ionized gas, $c_{\rm max}$: $u_{\rm IF} = c_0^2/2c_{\rm max}$. Spitzer (1968) has classified I-fronts through the isothermal sound speed in the neutral gas, c_0, and in the ionized gas, c_i. He defines the characteristic, D-critical velocity $u_D \equiv c_i - (c_i^2 - c_0^2)^{1/2} \simeq c_0^2/2c_i$, which gives the upper limit for the possible velocities of strong D-type fronts. Because of both adiabatic and atomic cooling in the ionized gas, $c_{\rm max}$ is larger than c_i; thus $u_{\rm IF} < u_D$. Kahn calculated that the gas leaves the I-front at about twice its isothermal sound speed and accelerates while expanding isothermally away from the cloud. He implicitly assumed that the cloud density at the surface, n_0, matches the density determined by the ionizing flux reaching the I-front, $F = \bar{\epsilon} F_i$ (where $\bar{\epsilon}$ corresponds to Oort and Spitzer's $1/f$, and F_i is the original direct Lyman continuum flux at the cloud location), and the propagation velocity of the I-front: $n_0 = F/u_{\rm IF}$; thereby pressure balance is guaranteed between the I-front and the cloud, and no pressure waves are driven into the cloud. Kahn therefore does not treat the evolution of a cloud when the star first turns on, since the initial cloud pressure, the absorption in the IBL, and the incident ionizing flux are unrelated quantities. As we shall show in this paper, the initial cloud pressure will generally be lower than the pressure exerted by the I-front, resulting in a shock driven into the initial cloud.

Dyson (1968, 1973) investigated self-gravitating isothermal globules which are exposed to an angular distribution of ionizing radiation. His globules are in hydrostatic equilibrium, and the I-front is assumed to propagate into the neutral gas at the D-critical velocity, thus not disturbing the gas through shock or expansion waves. He concluded that the cloud flattens in the direction of the maximum ionizing flux, trying to reach an equilibrium configuration under the influence of the boundary pressure. He could not treat the case of a planar radiation field, and also left out the dynamical evolution of a cloud when the ionization field first turns on.

Elmegreen (1976) studied the lifetime of clouds near OB stars and analyzed the effects of cloud photoevaporation on the structure of H II regions, but ignored the initially complex dynamical evolution of photoevaporating clouds. Using the results of Oort and Spitzer and of Kahn, he assumed the clouds to be at diameters constant in time and independent of the initial cloud density. McKee, Van Buren, and Lazareff (1984) generalized Elmegreen's treatment to include a range of cloud masses and made an approximate allowance for the initial compression by the shock.

The first fully time-dependent, axisymmetric radiation-hydrodynamic calculations of a cloud exposed to the ionizing radiation of an OB star were made by Klein, Sandford, and Whitaker (1980) and Sandford, Whitaker, and Klein (1982). Their numerical analysis follows the implosion of a neutral cloud adjacent to a larger cloud complex. The large compression they find is due both to shock focusing and to the rapid cooling of the shocked gas. Because of the coarse resolution it was not possible to follow the evolution beyond a shock crossing time; numerical studies never followed the cloud evolution beyond the initial implosion. The analytic theory introduced in this series of papers does take into account the effects of magnetic fields, shows how the large compression is due to a repeated shocking of the gas, and explains the evolution of imploding clouds over a larger time as well as for a wide range of values for the initial cloud parameters. We furthermore derive the cloud mass loss, velocity, and compression for a wide range of cloud parameters. All this is practically not derivable from single numerical simulations.

As most works on the photoevaporation of neutral clouds have pointed out, conditions at the I-front are of strong D-type, and a boundary layer of evaporating gas can shield the cloud from an exposure of the full ionizing flux of the star. The structure of both the I-front and the IBL has been studied for the case where the I-front is very thin compared with the dimension of the cloud, which implicitly demands $f \gg 1$. It has also been noted that the I-front may initially drive a shock into the cloud; the dynamical effects of this have not been studied quantitatively in previous works. So far it has not been possible to relate an initial population of clumps to the photoevaporating clumps observed in H II regions.

In this work we shall describe an approximate analytical solution for the evolution of photoevaporating clouds under the realistic assumption of axisymmetry. Under a wide range of conditions the problem is essentially specified by the initial cloud column density and the incident ionizing flux, expressed in terms of an ionization parameter at the location of the cloud. The effects of magnetic fields are taken into account in an approximate way.

We propose that the evolution of a neutral cloud subjected to the ionizing radiation of an OB star has two distinct stages. The first one, the *radiation-driven implosion* (also studied in dynamical calculations by Sandford, Whitaker, and Klein 1982; Klein, Whitaker, and Sandford 1985), will somewhat

depend on the internal structure and geometry of the initial cloud and is probably also subject to nonlinear three-dimensional dynamical behavior. Our analysis will make several simplifying assumptions, in the hope that we nevertheless capture the main aspects of the cloud evolution and derive reasonably accurate quantitative results. The initial cloud implosion is followed by an *equilibrium cometary* stage, in which the remaining cloud maintains a semistationary comet-shaped configuration, slowly evaporating while accelerating away from the ionizing star until the cloud has been completely ionized or reaches the edge of the H II region, or the ionizing star dies.

This work is divided into three papers. The present paper will focus on the radiation-driven implosion of a neutral cloud subjected to the ionizing radiation of a newly formed OB-type star. In § II we will introduce the parameters characterizing the initial cloud and study the effects of the ionizing radiation when the star first turns on. In § III we derive the structure of spherical I-fronts. Expanding on Kahn's analysis, we will drop the assumptions that the I-front be thin compared with the size of the cloud, that the gas in the IBL be in ionization and thermal equilibrium, and that the absorption of the incident ionizing flux herein be large ($f = 1/\bar{\epsilon} \gg 1$). The spherically symmetric results will be used in § IV to study the evolution of an ionization-shock front propagating into an initially spherical cloud. Since we are unable to integrate the hydrodynamic and radiation transfer equations simultaneously, we will derive approximate expressions for the I-front pressure on an axisymmetric convex surface and the evolution of the shock driven by the I-front. We will then estimate the mass lost in the implosion phase and the velocity of the remaining neutral cloud. In § V we estimate the structure of this postimplosion cloud, including the effects of an initial magnetic field. Finally, in § VI we derive some observable quantities for photoevaporating clouds in H II regions and, to apply our model in a very different environment, discuss the fate of intergalactic clouds when they are first exposed to the ionizing radiation of an AGN. Appendix C is a glossary of the symbols used in this paper.

In Paper II (Bertoldi and McKee 1990) we will show that after the initial radiation-driven implosion, the remaining cloud can settle into a steady, comet-shaped configuration, and we will discuss the cloud's structure, mass loss, lifetime, acceleration, and gravitational stability.

Paper III (Bertoldi *et al.* 1990) will present axisymmetric radiation-hydrodynamic numerical simulations to investigate the stability and importance of nonlinear dynamical effects in the evolution of photoevaporating clouds.

II. CLASSIFICATION OF PHOTOEVAPORATING CLOUDS

In this work, we introduce an approximate model for the evolution of an interstellar neutral clump which is exposed to the ionizing radiation of an early-type star. Since similar physical situations occur in quite different environments, we have tried to formulate our theory in a way that will make it easy to be applied to, e.g., intergalactic clouds exposed to the ionizing radiation of a nearby galaxy (Lyα clouds) or the small clouds suspected near the energetic central source of a quasar (broad emission line clouds). Even though the nature of the ionizing source and intercloud medium is very different in those cases, the basic parameters which in the subsequent discussion are adjusted to conditions in H II regions (cloud and intercloud sound speed and density) are easily modified. The calculation for the structure of ionization fronts (§ III) would have to be repeated if the ionizing radiation field has a power law instead of a blackbody spectrum, but would only modify the numerical fudge factors, not the general approach.

In this chapter we will outline the general theory for the radiation-driven implosion of a neutral clump by an ionizing star. Giant molecular clouds are observed to be inhomogeneous, with clumps having radii of up to several parsecs and densities between 600 and 2000 cm^{-3} embedded in an interclump medium (Pérault, Falgarone, and Puget 1985; Blitz 1987; Shu, Adams, and Lizano 1987). If these clumps are at a temperature of 10 K, they are at a pressure comparable to the mean pressure observed in atomic clouds not near H II regions, $n_i T_{i0} \sim 4000$ cm^{-3} K (Jura 1975). Here n_i is the interclump density and T_{i0} its temperature (unless specifically indicated by a subscript "H," "He," or "e," we shall use n as the number density of nuclei in the gas, counting both helium and hydrogen). In star-forming regions, the pressure can be as high as 10^4 cm^{-3} K. The observed typical magnetic field of 30 μG and turbulent velocity of order 1 km s^{-1} suggest that the total pressure in molecular clouds is significantly higher than the thermal pressure.

The neutral clumps, which contain a significant fraction of the mass but fill only a small fraction of the volume of such cloud complexes, are probably embedded in a tenuous, warm, maybe partially ionized intercloud gas. We shall assume that clumps in molecular clouds have typical densities of 1000 cm^{-3}. Atomic interstellar clouds have typical densities of 100 cm^{-3} at temperatures of around 100 K. Magnetic fields may in both types of clouds play an important role for the cloud pressure support.

For numerical estimates in the following analysis we shall consider higher density atomic clumps which are embedded in, and in pressure equilibrium with, a tenuous warm intercloud gas. An O- or B-type star which turns on in such an environment will, unlike a low-mass star, have a profound effect on it. After disrupting the dense clump that gave birth to the ionizing star, its radiation will drive a rapid weak R-type I-front (the classification of I-fronts is taken from Kahn 1954 and Spitzer 1968) into the surrounding gas (e.g., Spitzer 1978, p. 249). The tenuous interclump gas will get heated to a temperature of $\sim 10^4$ K and ionized out to its Strömgren radius $R_{St} = 72.4(S_{49}/n_i^2)^{1/3}$ pc, where $S = 10^{49} S_{49}$ s^{-1} is the star's emission rate of photons beyond the Lyman limit.

Since the neutral clumps are at higher densities than the intercloud medium (ICM), the ionization front will penetrate the clumps with a significantly lower velocity. Our aim is to understand the fate of a clump from the time when the R-type I-front ionizing the ICM engulfed the clump with ionized gas and thereby exposed it to the ionizing radiation of the star. The dynamical impact of the ionizing radiation will dominate the future evolution of the clump. The interclump gas may also affect the dynamical evolution of the clump, since it is at a higher pressure in its ionized state and may therefore drive a shock wave into the radiation-shielded back side of the clump. Since the actual pressure difference between the ICM and the neutral gas depends on many factors (the heating of the ICM, the heating of the clump by the far-UV radiation of the ionizing star, and the importance of the magnetic pressure), we shall for simplicity neglect its direct dynamical impact on the neutral clump.

We shall also neglect possible initial pressure or density gradients within the neutral clump and assume an initially spherical shape, and either no magnetic field or a well-ordered one.

We can now study the evolution of one such clump of initial radius r_0, density ρ_0, and temperature T_0, which is subject to the ionizing radiation of a single OB star (or a compact group) at a distance $R_0 > r_0$.

a) *Initial Cloud Parameters*

In this section we introduce the parameters which characterize and classify the initial clouds. We can express the maximum column density in an initial cloud through the dimensionless parameter

$$\eta \equiv \frac{\alpha_i r_0 n_0}{c_i} = \frac{r_0 n_0}{4.40 \times 10^{18}\ \mathrm{cm}^{-2}} = 702 r_{0,\mathrm{pc}} n_{0,3} . \quad (2.1)$$

Here $n_0 = 10^3 n_{0,3}$ is the number density of nuclei in the neutral cloud (counting both H and He nuclei), $\alpha_i = 2.59 \times 10^{-13} T_{i,4}^{-0.85}$ is the rate coefficient for hydrogen recombinations to all but the ground state, $c_i = 11.4 T_{i,4}^{1/2}$ km s^{-1} is the isothermal sound speed in the ionized interclump gas, and $r_{0,\mathrm{pc}} = r_0/1$ pc. For numerical estimates we have assumed that $T_{i,4} = 1$. The cloud has a visual extinction $\bar{A}_V = 2.0 \times 10^{-3} \eta \delta_{\mathrm{gr}}$, where δ_{gr} is the ratio of the extinction per hydrogen nucleus in the cloud to the standard value given by Spitzer (1978).

Ignoring the attenuation through absorption by the intercloud gas, the Lyman continuum flux at a distance R_0 from the ionizing source is

$$F_i = \frac{S}{4\pi R_0^2} = 8.36 \times 10^{10} \frac{S_{49}}{R_{0,\mathrm{pc}}^2}\ \mathrm{s}^{-1}\ \mathrm{cm}^{-2} . \quad (2.2)$$

We shall consider the point on the cloud surface closest to the star. If the incident Lyman continuum flux here is such that conditions are M-type (i.e., $u_D < F_i/n_0 < 2c_i$, where $u_D \simeq c_{\mathrm{I}}^2/2c_i$ is the D-critical velocity and $c_{\mathrm{I}} \simeq c_0$ is the isothermal sound speed in the neutral gas just ahead of the I-front), the I-front drives a shock into the neutral gas, compressing it to such a pressure that conditions right at the I-front are approximately D-critical (i.e., $F_i \simeq n_{\mathrm{I}} u_D$, where n_{I} is the compressed gas density just ahead of the I-front). The initial shock velocity at the symmetry axis, v_{s0}, is found approximately by equating the shock ram pressure $\rho_0 v_{s0}^2$ to the total (dynamical plus thermal) pressure at the D-critical I-front, where $n_{\mathrm{I}} c_{\mathrm{I}}^2 = 2F_i c_i$:

$$v \equiv \frac{v_{s0}}{c_i} = \left(\frac{2F_i}{n_0 c_i}\right)^{1/2} = 12.1 \left(\frac{S_{49}}{R_{0,\mathrm{pc}}^2 n_{0,3}}\right)^{1/2} . \quad (2.3)$$

We have implicitly assumed that the sound speed in the initial cloud is much smaller than in the ionized gas, $c_0 \ll c_i$, so that strong shock jump conditions apply. This also ensures that the acceleration of the evaporating gas by the cloud's self-gravity is unimportant, since the cloud escape velocity is typically of order c_0.

The dimensionless velocity v can be related to an ionization parameter

$$\Gamma \equiv \frac{F_i}{n_0 C} = 2.79 \times 10^{-3} \frac{S_{49}}{R_{0,\mathrm{pc}}^2 n_{0,3}} \quad (2.4)$$

through $\Gamma = 1.90 \times 10^{-5} T_{i,4}^{1/2} v^2$. Here C is the speed of light. As ionized gas streams radially away from the I-front, part of the incident ionizing flux will get absorbed in an ionized boundary layer, as first noticed by Oort and Spitzer (1955). If $q \equiv F_i/(u_{\mathrm{IF}} n_{\mathrm{I}})$ is the ratio of the incident ionizing photon flux to the ionized gas flux evaporating off the I-front (for $q \gg 1$ this is equivalent to the ratio of the incident photon flux to the photon flux reaching the I-front; thus q corresponds to f in Oort and Spitzer 1955 and $1/\bar{\epsilon}$ in Kahn 1969), in a steady state the shock velocity will be reduced to

$$v_s = \frac{v c_i}{(\phi_D q)^{1/2}} , \quad (2.5)$$

where ϕ_D is a fudge factor of order unity to be computed in § III.

To compute q for a given cloud, we have to integrate the absorption of ionizing photons along the line connecting the I-front with the star. We shall introduce the photoevaporation parameter

$$\psi \equiv \frac{\alpha_i F_i r_0}{c_i^2} = \frac{v^2 \eta}{2} = 5.15 \times 10^4 \frac{S_{49} r_{0,\mathrm{pc}}}{R_{0,\mathrm{pc}}^2} , \quad (2.6)$$

which can be physically interpreted as the number of recombinations a single hydrogen atom would undergo if it had to cross a cloud radius r_0 at the typical expansion velocity of the evaporating gas, c_i, while in an ionized gas that is at the density of the evaporating gas (if all of the incident Lyman continuum photons reached the cloud surface to ionize a new cloud atom), F_i/c_i. A large value of ψ implies that the gas streaming off the I-front does recombine rapidly, so that some of the incident photons are absorbed in the IBL. A small value of ψ implies that recombinations of the evaporating gas are not important; thus all the Lyman continuum photons reach the I-front.

A simple calculation as outlined in, e.g., Spitzer (1978, p. 264) shows that q is related to ψ approximately through $q(q-1) \simeq \omega\psi$, where ω is $\frac{1}{3}$ in Spitzer, but can be determined more accurately as shown later in § III. It is seen that q is large if the recombination length in the IBL is small compared with the cloud radius: If $n_{\mathrm{II}} \equiv F_i/(qc_i)$ is a typical density at the I-front, then $l_r/r_0 = \psi/q = \omega/(q-1)$ is the recombination length relative to the cloud radius. We shall note that the absorption length, $l_a \sim 1/(n_{\mathrm{II}} \bar{a})$, is typically much smaller than the recombination length, so that the I-front itself is very thin compared with the cloud radius if q is large. Here $\bar{a}$ is a frequency-averaged hydrogen absorption cross section. When $\psi < 10$ and $q \simeq 1$, the recombination length becomes comparable to or larger than the cloud radius. Therefore, only few incident Lyman continuum photons get absorbed in the IBL. Since $l_a/r_0 \sim 1/(r_0 n_{\mathrm{II}} \bar{a}) \sim q/\psi$, the I-front widens roughly as ψ^{-1} for small ψ.

If the initial ionizing flux at the cloud surface is large enough to make conditions here R-type (i.e., if $F_i > 2c_i n_0$), a rapid R-type I-front will move into the cloud without dynamically perturbing the neutral gas. As the I-front propagates into the cloud, the increasing column of dense recombining (and thereby absorbing Lyman continuum photons) gas it creates will steadily reduce the flux that reaches the front, until conditions here become M-type and the I-front starts driving a shock into the neutral upstream gas. Up to this point, the I-front has ionized a gas layer of thickness $2r_0\delta$, measured parallel to the planar radiation field, where

$$\delta = \frac{F_i - 2c_i n_0}{2r_0 n_0^2 \alpha_i} = \frac{v^2 - 4}{4\eta} . \quad (2.7)$$

We shall further define

$$\delta' \equiv \frac{v^2}{4\eta} = 5.23 \times 10^{-2} \frac{S_{49}}{n_{0,3}^2 r_{0,\mathrm{pc}} R_{0,\mathrm{pc}}^2} \quad (2.8)$$

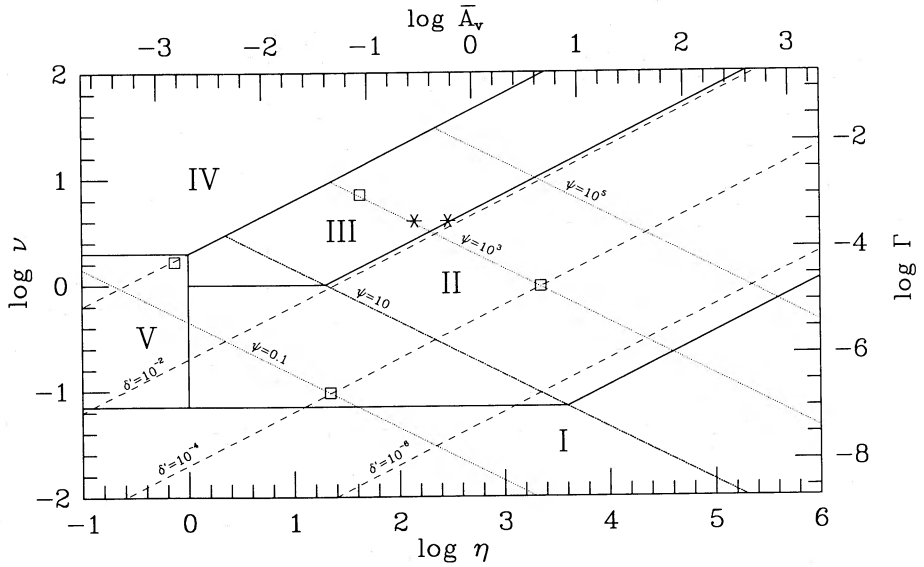

FIG. 1.—Initial cloud parameter space as discussed in § II*b*: ν and Γ are parameters describing the relative density of the ionizing radiation field at the cloud position and the initial cloud gas density; Γ can be interpreted as an ionization parameter, whereas ν is a measure for the initial I-front–driven shock velocity; $\eta = r_0 n_0/(4.4 \times 10^{18}\ \mathrm{cm}^{-2})$ is the dimensionless initial cloud column density; and $\bar{A}_V$ is the mean visual extinction of the cloud. For clouds in region I the incident ionizing flux has a negligible dynamical effect on the cloud; clouds in region I are usually not found inside H II regions. Clouds in region II will be compressed by an ionization-shock front. The shock velocity is limited to c_i for clouds in region III. Clouds in region IV will be ionized completely by the initial R-type I-front. Clouds in region V do get compressed by an IS-front, but their evolution is intrinsically time-dependent. The parameter ψ is a measure for the absorption efficiency of the photoevaporating gas: for $\psi \gg 10$, most of the incident photons get absorbed before reaching the I-front. The parameter δ' is the width of the instantly ionized cloud layer relative to the cloud diameter. The open squares indicate the locations of the clouds displayed in Fig. 8: *left*, Fig. 8*a*; *lower*, Fig. 8*b*; *top*, Fig. 8*c*; *right*, Fig. 8*d*. The line dividing region I from regions II and V is for an initial cloud temperature of 100 K or a magnetic field with $b = 0.6$. The stars refer to two example clouds of 1 and 10 solar masses 10 pc from the center of the Rosette Nebula.

as the relative width of the layer of ionized gas at initial cloud density in which the gas recombinations would exactly balance the incident Lyman continuum flux.

b) Initial Cloud Parameter Space

We shall classify an initial cloud through two dimensionless parameters: η, the cloud column density, and ν, the initial shock velocity (equivalently, the ionization parameter). The observationally interesting part of the initial cloud parameter space defined by these parameters is displayed in Figure 1. In parameter space we distinguish several regions (numbered I–V and separated by heavy solid lines), each representing clouds with qualitatively distinct evolutions. The heavy dotted line in Figure 1 separates clouds for which a steady IBL will absorb a significant fraction of the incident ionizing radiation (*above*: $\psi > 10$) from clouds for which an insignificant amount of radiation is absorbed in the IBL (*below*: $\psi < 10$). For the latter clouds, the recombination length and eventually the absorption length in the gas streaming off the neutral cloud become comparable to the radius of the cloud. The I-front cannot be assumed thin, and detailed calculations are necessary to determine the flow pattern and the pressure exerted on the neutral gas. We have undertaken such calculations in § III under the assumption that the I-front propagates into the neutral cloud at a velocity small compared with c_i. The historic works referenced in § I limited themselves to clouds for which $\psi \gg 1$, i.e., $q \gg 1$.

In case the cloud magnetic field provides a significant fraction of the cloud pressure, the isothermal sound speed in the neutral cloud is to be replaced by the isothermal magnetosonic speed defined as $c_0^2 \equiv p_{\mathrm{th}}/\rho_0 + v_A^2/2$, where p_{th} is the thermal gas pressure and $v_A \equiv B_0/(4\pi\rho_0)^{1/2}$ is the Alfvén velocity in the initial cloud.

i) *Region I: Clouds Unaffected*

For clouds in region I, conditions at the I-front are D-type with respect to the initial cloud (i.e., $F_i < u_D n_0$). For $\psi < 10$ this implies $\nu < (T_0/2T_i)^{1/2}$; the line separating region I from region II is drawn for $T_0 = 100$ K. For clouds below this line, the I-front cannot produce a pressure sufficient even to confine the initial cloud. Since we can assume that the initial cloud was in pressure equilibrium with the intercloud gas, the newly ionized gas will not be able to expand freely into the ICM, and the flow pattern of the photoionized gas will depend mostly on the intercloud pressure and density. A steady state cannot be achieved in such an evaporation flow. Overall, the incident ionizing radiation will have a negligible dynamical effect on the cloud, which will evaporate at a rate of less than $\pi r_0^2 F_i$ hydrogen atoms per second. Clouds under those conditions are usually not found inside H II regions if the cloud and intercloud medium were initially in pressure equilibrium. If c_{i0} is the initial intercloud gas sound speed, then the distance from the ionizing star at which the weak R-type I-front in the intercloud gas becomes R-critical, R_R, is usually smaller than the distance R_D at which conditions at the cloud surface turn D-critical. Provided that the intercloud gas is not initially ionized,

$$\frac{R_D}{R_R} \simeq \frac{2c_i}{c_{i0}} > 1 \,. \tag{2.9}$$

On the other hand, the I-front initially driven into the ICM usually becomes R-critical very close to the Strömgren radius (e.g., Spitzer 1978, p. 250). Therefore, conditions such as those in region I are usually not found inside H II regions.

If the initial cloud pressure is dominated by its magnetic field, which can be related to the cloud density through $B_0 = 10^{-6} b n_0^{1/2}$ (where b is a factor of order unity), then conditions at the cloud surface are D-type initially if $v < 0.12bq^{1/2}$. For $b = 0.6$, conditions are D-type initially for clouds below the lower heavy line in Figure 1.

ii) *Region II: Ionization-Shock Front Cloud Implosion*

Clouds in region II will be compressed by an ionization-shock front (IS-front). At the symmetry axis, the velocity with which the IS-front propagates into the cloud is initially $v_s = vc_i$, and after a steady flow of ionized gas off the I-front has established an IBL which absorbs a fraction of the incident flux, the velocity is reduced to the value given by equation (2.5). The ionized gas streams off the neutral shocked gas layer with a flow pattern which can be considered steady and is described in detail in § III. The neutral gas is ionized in a layer on the cloud surface that we denote the ionization front. For clouds with $\psi \gg 1$, the I-front is thin compared with the size of the initial cloud. For $\psi < 1$, where almost none of the incident ionizing radiation is absorbed by the recombining gas streaming off the I-front, the I-front can extend out a significant fraction of the I-front's radius of curvature. Only for large ψ (or, equivalently, large q) can the I-front be considered thin enough to justify a plane-parallel approximation as applied by, e.g., Kahn (1969).

For clouds where $v_s \simeq c_i$, the shock velocity becomes comparable to the velocity to which the ionized gas is accelerated in (and relative to) the I-front. Since the IBL extends out effectively 20%–30% of the radius of curvature of the I-front, the time scale for a significant change in the radius of curvature of the I-front is then comparable to the adjustment time of the flow in the IBL, and a steady ionized gas flow is no longer possible.

iii) *Region III: Velocity Limiting for Strong Ionization-Shock Fronts*

Region III represents clouds for which the velocity of the IS-front (eq. [2.4]) would exceed c_i. The gas leaving the I-front is then approximately at rest in the rest frame of the initial cloud. A layer of ionized, recombining gas will shield the I-front in such a way that the velocity of the front is limited to the velocity with which this layer can expand away into the ICM. Since the velocity with which a rarefaction wave can propagate into the layer is c_i, this is also the maximum possible velocity of the IS-front. A larger velocity would lead to a buildup of the dense layer of ionized gas, which would reduce the ionizing flux that drives the IS-front velocity, thereby limiting the shock velocity to c_i.

iv) *Region IV: Cloud Zapping*

A cloud in region IV will be ionized completely (or "zapped") by the initial rapid R-type I-front. Then the cloud is at a significantly higher pressure and density than the intercloud gas and will expand into the ICM in a sound crossing time $\sim 2r_0/c_i$. The line separating region IV from region III indicates clouds for which $\delta = 1$.

v) *Region V: Nonequilibrium Evaporation Fronts*

For clouds in region V an equilibrium I-front would contain a mass which is equal to or larger than the mass of the initial cloud. A steady state I-front can therefore not be established before the I-front–driven shock has swept over all of the initial cloud. The cloud evolution in this region is therefore intrinsically time-dependent.

III. THE STRUCTURE OF STEADY SPHERICAL IONIZATION FRONTS

Concave spherical I-fronts as edges of H II regions have been studied by, e.g., Goldsworthy (1961) and Axford (1961), but are in many important aspects significantly different from convex ionization-shock fronts of photoevaporating clouds. Mendis (1969) computed the structure of spherical I-fronts for a spherically symmetric radiation field. He concluded that conditions at the front could be either strong D-type or D-critical, depending on the spectral type of the incident radiation. Planar IS-fronts were first studied and classified by Kahn (1954). The energy equation he used is not realistic, and we shall adopt the classification suggested by Spitzer (1968), which gives the maximum possible velocity of a strong D-type I-front, $u_D = c_i - (c_i^2 - c_I^2)^{1/2}$, in terms of the equilibrium temperatures upstream and downstream of the I-front. Kahn (1969) investigated the photoevaporation of spherical clouds embedded in an isotropic radiation field. He assumed that the I-front embracing a cloud is thin compared with the cloud radius and can therefore be treated like a planar front. In his approximate analytical derivation for the structure of planar I-fronts, he showed that a steady solution is possible if the ionized gas is able to expand freely into the intercloud medium. The speed with which the I-front propagates into the upstream neutral gas is determined by the isothermal sound speed in the neutral gas (and, in the case of a magnetic field, the isothermal magnetosonic speed), c_I, and the maximum isothermal sound speed in the evaporation flow, c_{max}, which is reached at the isothermal sonic point: $u_{IF} = c_{max} - (c_{max}^2 - c_I^2)^{1/2} \simeq c_I^2/2c_{max}$, provided that $c_{max} \gg c_I$, which is usually the case. Since recombinations are insignificant in the I-front, for thin I-fronts the ionizing flux F that reaches the front is approximately equal to the material flux leaving the front, and the density of the neutral gas upstream of the I-front, n_I (counting H and He nuclei), is given by $n_I = F/u_{IF}$ for a steady flow. If the initial cloud density, n_0, is lower than this value, a shock will precede the I-front, increasing the density to the value required for a steady front. The proper velocity with which the I-front moves into the initial cloud is then equal to the postshock neutral gas velocity plus u_{IF}. In the unusual case where $n_I < n_0$, a rarefaction wave has to precede the I-front. Kahn further estimated that the isothermal Mach number of the ionized gas increases toward an asymptotic value of approximately 2, depending somewhat on the gas cooling rates and the spectral type of the ionizing star. Kahn used this value as the terminal Mach number of the spherically diverging evaporation flow (which was assumed isothermal and in ionization equilibrium) off a spherical, photoevaporating cloud. Note that this implies that the proper velocity of the I-front with respect to the cloud is much smaller than the velocity with which the gas leaves the I-front. With this implicit assumption and the assumption that the front be thin compared with the size of the cloud, Kahn limited his analysis to clouds which are in the $\psi \gg 1$ part of region II in Figure 1.

To expand on Kahn's analysis, in this section we shall derive the detailed structure of steady, spherical ionization fronts, dropping both the assumptions that the front be thin and that it be in thermal and ionization equilibrium. The I-front itself is not treated in the planar approximation, and the temperature and ionization of the gas, as well as the transfer of the ionizing radiation, are treated in a self-consistent manner. We do assume that the gas streams along surface normals (keeping the problem one-dimensional) and impose the on-the-spot approx-

imation for ground-state recombination photons. This is obviously a justified approximation in the case where most of the incident ionizing photons are absorbed in the IBL. In the other extreme, when $q \simeq 1$ and the IBL is "optically thin" to the Lyman cotinuum photons, the recombinations are not important and the error made in the recombination rate is therefore insignificant. Like Kahn, we still assume that the proper velocity of the I-front is small, so that the time scale for a significant change in the radius of curvature of the I-front is much greater than the adjustment time of the flow. Only then can the flow be stationary.

Our analysis breaks down if the ionizing spectrum contains a large flux of hard UV photons and X-rays which can heat the gas to 10^4 K without ionizing it. Then a heating front propagates into the cloud ahead of the I-front and causes the expansion of the neutral warm gas.

a) Geometry

We shall investigate the flow off a spherical cloud of density n_0, temperature T_0, and radius r_0, along the line of sight connecting the ionizing star with the cloud center. The cloud is composed of atomic hydrogen and helium at densities $n_{\rm H}$ and $n_{\rm He}$, respectively, with $n = n_{\rm H} + n_{\rm He}$. Since the I-front is likely to drive a shock or rarefaction wave into the cloud, the density upstream of the I-front, $n_{\rm I}$, is different from the initial cloud density, n_0. If r is the radial coordinate originating at the cloud center, then at r_0 the optical depth toward the ionizing star will decrease rapidly with increasing r, as the Lyman continuum flux, the gas ionization, the velocity, and the temperature increase. The cloud radius is assumed small compared with its distance to the ionizing star, so that the ionizing radiation field is plane-parallel at the cloud location. We shall make the simplifying assumption that the ionized gas streams along straight lines perpendicular to the cloud surface (Dyson 1973). We will compute the flow in the rest frame of the I-front and assume that the curvature of the surface remains constant for a time sufficient for an adjustment to a quasi-steady state. The velocity of the I-front, i.e., the velocity with which the neutral gas enters the I-front, will be computed and expressed in terms of a characteristic D-critical velocity, $u_D \equiv c_{\rm I}^2/2c_i$: $u_{\rm IF} = \phi_D u_D$, which defines the dimensionless velocity parameter ϕ_D. This parameter accounts for the difference between c_i and $c_{\rm max}$ as well as for the effects of spherical divergence when the I-front is not thin compared with its radius of curvature. The ionized gas has the radial velocity $v(r)$ which steadily increases with r. We will compute steady solutions to the gas flow, i.e., all partial time derivatives in the gas and radiation equations are set to zero.

b) Fluid Equations

Let $n_{\rm H}$ be the number density of hydrogen nuclei per unit volume, $X_{\rm He} = n_{\rm He}/n_{\rm H}$ the relative abundance of helium to hydrogen, $x_{\rm H} = n_p/n_{\rm H}$, and $x_{\rm He} = n[{\rm He}^+]/n_{\rm He}$ the hydrogen and helium ionization, respectively. The ionization of He^+ to He^{++} is negligibly small (unless the ionizing radiation field is extremely hard, as for power-law spectra) and shall for simplicity be ignored. The gas mass density is $\rho = \mu_{\rm H} n_{\rm H}$, where $\mu_{\rm H} \equiv (1 + 4X_{\rm He})m_{\rm H}$ is the mean mass per hydrogen nucleus, and the electron density is $n_e = n_{\rm H}(x_{\rm H} + x_{\rm He} X_{\rm He})$. The adiabatic sound speed in the gas is given by

$$c = \left\{\frac{5}{3}\frac{kT}{\mu_{\rm H}}\left[1 + x_{\rm H} + (1 + x_{\rm He})X_{\rm He}\right]\right\}^{1/2} \tag{3.1}$$

and the isothermal sound speed by $(\frac{3}{5})^{1/2}c$. We further use $c_i = 11.4$ km s^{-1} as a characteristic isothermal sound speed in the ionized gas (i.e., $T_i = 10^4$ K). The steady-flow continuity equation in spherical geometry is written

$$\frac{d}{dr}(r^2 \rho v) = 0 \tag{3.2}$$

and yields $r^2 \rho v =$ constant. The momentum equation, neglecting the gravitational acceleration by the neutral cloud, is

$$v\frac{dv}{dr} = -\frac{1}{\rho}\frac{dp}{dr}, \tag{3.3}$$

with p being the thermal gas pressure. We do not include the cloud's gravity and therefore have to make sure in future applications that the escape velocity at the cloud surface is much smaller than c_i. The total heating due to the ionization of hydrogen and helium shall be written $n_{\rm H}\Gamma_h$, and the total cooling due to inelastic collisions and electronic recombinations $n_{\rm H} n_e \Lambda$ (ergs cm^{-3} s^{-1}). The energy equation can then be written

$$\rho v \frac{d}{dr}\left(\frac{1}{2}v^2 + \frac{5p}{2\rho}\right) = n_{\rm H}(\Gamma_h - n_e\Lambda). \tag{3.4}$$

Combining equations (3.2)–(3.4), we can rewrite the momentum and energy equations as differential equations for the velocity and the adiabatic sound speed:

$$\frac{dv}{dr} = \frac{1}{v^2 - c^2}\left[\frac{2vc^2}{r} - \frac{2(\Gamma_h - n_e\Lambda)}{3\mu_{\rm H}}\right], \tag{3.5}$$

$$\frac{3v}{2}\frac{dc^2}{dr} = \frac{\Gamma_h - n_e\Lambda}{\mu_{\rm H}} + \frac{2}{1 - c^2/v^2}\left(\frac{\Gamma_h - n_e\Lambda}{3\mu_{\rm H}} - \frac{c^2 v}{r}\right). \tag{3.6}$$

c) Ionizing Radiation Field

The Lyman continuum flux incident on the photoevaporating cloud is assumed to emerge from a blackbody of surface temperature T_* and is divided into two parts, below and above the helium ionization edge at 1.808 rydbergs. Since there is a direct correspondence between the remaining flux in each part and the spectral shape therein, we have computed mean absorption rate coefficients and photoelectron excess energies as functions of $F_1/F_{1,i}$ and $F_2/F_{2,i}$. Here F_1 and F_2 are the ionizing fluxes in the energy ranges below and above the He edge at a given point in the photoevaporating gas flow, and the $F_{k,i}$ are the direct incident fluxes without absorption by the ionized gas. Note that $F_i = F_{1,i} + F_{2,i}$ is given by equation (2.2). We have solved the hydrodynamic equations together with the four equations for the hydrogen and helium ionization and the ionizing photon fluxes F_1 and F_2. The hydrogen ionization equation is coupled to the helium ionization through the helium ground state recombinations and the (2, 1) bound-bound transition photons which can ionize hydrogen. We have applied the on-the-spot approximation, i.e., all reionizing recombination photons are absorbed by the gas at the same location. The ionization and flux equations used are described in Appendix A. With $x_e \equiv n_e/n$ as the total gas ionization and $F = F_1 + F_2$, we can combine the ionization equations (A3) and get an equation for the gas ionization:

$$nv\frac{dx_e}{dr} = \frac{dF}{dr} - n_p n_e \alpha_{\rm BH}, \tag{3.7}$$

where α_{BH} is the excited state H electronic recombination rate coefficient. The small coupling term due to the helium recombination photons was neglected. We define

$$q \equiv \frac{F_i}{n_I u_{IF}} \tag{3.8}$$

as the ratio between the incident flux of ionizing photons and the flux of ionized gas streaming off the I-front. If $q \gg 1$, this is equivalent to the ratio between the incident flux and the flux that actually reaches the I-front and expresses how much flux has been absorbed in the layer of ionized gas due to the reionization of recombining gas. A large value of q indicates that only a small fraction of the incident ionizing radiation directly ionizes the neutral cloud, whereas most is absorbed in the recombining gas in the ionized boundary layer. For given element abundances, the solution to the hydrodynamic equations is a one-parameter set, the free parameter being the photoevaporation parameter ψ (eq. [2.6]). With $n_{II} \equiv n_I u_{IF}/c_i$ as a typical density of the ionized gas in the I-front, we can integrate equation (3.7) from $r < r_0$, where the ionization and ionizing flux have dropped to an insignificant amount, out to some large $r \gg r_0$, where the ionizing flux reached its initial value, F_i. This yields

$$\phi_q = q - \frac{\psi\omega}{q} \rightarrow q(q - \phi_q) = \psi\omega\,, \tag{3.9}$$

with the dimensionless parameters

$$\phi_q \equiv \int \left(\frac{r_0}{r}\right)^2 dx_e\,, \tag{3.10}$$

$$\omega \equiv \int \frac{n_e n_p}{n_{II}^2} \frac{\alpha_{BH}}{\alpha_i} \frac{dr}{r_0}\,. \tag{3.11}$$

Here ϕ_q describes the thickness of the ionization front, i.e., the region where the evaporating gas is first ionized; the thickness of the I-front is approximately $(1 - \phi_q)$ times the radius of curvature of the front, r_0. The parameter ω is the effective fractional thickness of the recombination layer, i.e., the region which absorbs incident photons through the reionization of recombining gas. In a column of unit cross section connecting the ionizing star with the cloud, $\omega n_{II}^2 \alpha_i$ hydrogen atoms recombine to states other than the ground state per second, and in ionization equilibrium an equal number of incident Lyman continuum photons are being absorbed. Our calculations show (§ III*f*) that ω ranges between 0.2 for $\psi \ll 1$ and 0.1 for $\psi \gg 1$. In the simplified case of an isothermal, fully ionized evaporation flow emerging at r_0 with its radial velocity equal to the isothermal sound speed c_i, $\omega = 1/[3(1 + X_{He})]$ and $\phi_q = 1$ (compare, e.g., Spitzer 1978, eq. [12-35], where $X_{He} = 0$).

d) Heating and Cooling

If the cloud hydrogen is initially molecular, the FUV radiation of the ionizing star will photodissociate the gas upstream of the I-front (Tielens and Hollenbach 1985). We shall therefore assume that the I-front propagates into atomic gas. When ionized, the gas is heated through the thermalization of photoelectrons created by hydrogen ionizations below, and both hydrogen and helium ionizations above, the helium ionization edge. The ionizations of H by He ground state as well as $n = 2$–1 recombination photons also contribute to the gas heating, whereas each hydrogen recombination removes an energy of approximately $0.7kT$ per recombination (Spitzer 1978). The most prominent cooling in the I-front is due to the collisional excitation of neutral hydrogen. The collisional excitation of fine structure and metastable levels in C, N, O, Si, S, and Fe is an important cooling mechanism of the photoionization heated gas. Since we cannot easily compute the correct ionization structure for all of those elements, we have, besides H and He, included only those for which the ionization does not change significantly within the I-front or, as in the case of oxygen, is collisionally coupled to that of hydrogen. The ignored higher ionization states (e.g., O III) will contribute to the cooling in the outer parts of the IBL, but at higher optical depth they should be less important for the thermal balance in the I-front. In our model calculations we have assumed a cosmic abundance (6.3×10^{-4}) of oxygen and in one case included once-ionized silicon at an abundance of 3.2×10^{-5} (Spitzer 1978). The oxygen cooling is assumed to be due to the excitation of the ^3P level in O I and the ^4S level in O II, and the Si cooling is assumed due to the $^2P_{1/2 \rightarrow 3/2}$ and $^2P \rightarrow {}^4P$ transitions. The cooling rates and the coupling coefficient for the oxygen ionization are taken from Dalgarno and McCray (1972). Adding up all the contributions yields the total cooling rate as a function of the gas temperature, H, and He ionization.

e) Numerical Method

Equations (3.5), (3.6), (A2), and (A3) form a system of coupled first-order differential equations for the six main parameters we used to describe the structure of a spherical ionization front: c, the adiabatic sound speed, v, the radial velocity of the gas, x_H, x_{He} the ionization of hydrogen and helium, and F_1, F_2 the ionizing photon flux below and above the helium ionization edge.

Both the momentum and energy equations are singular at the sonic point, which makes it difficult to integrate them numerically. We found that the substitution for v of a new variable can at least remove the singularity in the momentum equation. Adopting an idea advanced by Melia (1988) for a similar problem, the new variable substituted for the gas velocity is

$$\varphi \equiv \frac{1}{2}\left(\frac{v}{c} + \frac{c}{v}\right) \Rightarrow \frac{v}{c} = \varphi \mp (\varphi^2 - 1)^{1/2}\,. \tag{3.12}$$

The momentum equation, rewritten in terms of the new variable, is nonsingular:

$$\frac{d\varphi}{dr} = \frac{1}{3v^2 c}\left[\frac{vc^2}{r}\left(3 + \frac{v^2}{c^2}\right) - \frac{\Gamma_h - n_e \Lambda}{6\mu_H}\left(3 + 5\,\frac{v^2}{c^2}\right)\right]. \tag{3.13}$$

We are still left with the singularity in the energy equation. Since neither the position nor the values for the variables at the singular adiabatic sonic point are known in advance, we have to integrate the differential equations outward and iteratively determine the initial values that lead to both a smooth transition at the sonic point (the transition from the subsonic to the supersonic branch is made by switching the sign in equation (3.12) from minus to plus when $d\varphi/dr = 0$) and the correct value for the incident ionizing flux far out. The initial values chosen for the variables at the inner boundary, r_0, were $T_1 = 100$ K, $F_1 = 10^{-5} F_{1,i}$, and, for the ionization, $x_H = x_{He} = 10^{-4}$. The results are insensitive to these inner boundary values. The upstream neutral gas density is then given through

$$n_I = \frac{F_i}{\phi_D u_D q}\,. \tag{3.14}$$

TABLE 1

IONIZATION FRONT MODEL CALCULATIONS

Model	X_{He}	O	ψ	q	ϕ_D	$1-\phi_q$	ω
1	0	1	0.239	0.58	2.21	0.487	0.153
2	0	1	0.399	0.71	1.86	0.385	0.172
3	0	1	0.797	0.90	1.55	0.265	0.186
4	0	1	4.05	1.38	1.22	0.102	0.161
5	0	1	10.1	1.79	1.14	0.064	0.150
6	0	1	40.5	2.88	1.09	0.035	0.136
7	0	1	405	7.53	1.04	0.016	0.122
8	0.1	1	0.304	0.65	2.09	0.440	0.197
9	0.1	1	0.507	0.79	1.80	0.345	0.212
10	0.1	1	1.01	0.99	1.53	0.238	0.218
11	0.1	1	5.15	1.52	1.25	0.099	0.179
12	0.1	1	12.9	1.98	1.18	0.063	0.159
13	0.1	1	51.5	3.24	1.12	0.037	0.142
14	0.1	1	515	8.51	1.09	0.021	0.123
15	0	0	4.05	1.35	1.17	0.097	0.148
16	0	0	40.5	2.74	1.02	0.030	0.119
17	0	0	405	6.88	0.95	0.012	0.100
18[a]	0	1	0.399	0.60	1.88	0.468	0.095
19[a]	0	1	0.797	0.78	1.56	0.341	0.115
20[a]	0	1	4.05	1.27	1.22	0.141	0.128
21[a]	0	1	40.5	2.77	1.08	0.048	0.124
22[a]	0	1	405	7.24	1.02	0.020	0.112
23	0.1	1	51.5	3.08	1.09	0.040	0.126
24	0.1	0	51.5	2.30	1.01	0.030	0.178
25[b]	0	1	40.5	3.07	1.10	0.026	0.158

[a] For O5 star.

[b] With Si cooling.

The parameters ω, ϕ_D, and ϕ_q (and with helium, the inner boundary value for F_2/F_1) are found iteratively by integrating the equations in such a way that the solution is smooth at the sonic point and both F_1 and F_2 approach their initial values $F_{1,i}$ and $F_{2,i}$ at the outer integration limit. The equations were integrated numerically from r_0 to $4r_0$, using a high-order Runge-Kutta scheme.

f) Results

In Table 1 we have listed the input parameters and the numerically determined I-front factors for several model calculations. In Figures 2 and 3 we plot ϕ_D, ϕ_q, and ω as functions of ψ for different cooling metal abundances with and without helium. Figures 4–6 show the structure of several example model ionization fronts.

We can summarize the results obtained from our model calculations as follows:

1. The I-front parameters ϕ_D and ϕ_q do not change significantly over several orders of magnitude for $\psi > 1$ and can be set approximately equal to unity. The thickness of the I-front is reflected in the deviation of ϕ_q from unity. For $\psi < 1$, corresponding to clouds which are small and/or far from the ionizing source, the width of the I-front can be a significant fraction of the radius of curvature of the I-front. In this case q can become smaller than unity, which means that the effective cross section of the cloud to the ionizing radiation increases beyond its geometric cross section, and there is a significant change in the dependency of ϕ_D and ϕ_q on ψ. For these clouds the ionized gas streaming off the I-front is severely out of ionization and thermal equilibrium, i.e., the recombination length is not small compared with the cloud radius. The ionized boundary layer is ineffective in shielding the cloud from the incident ionizing photons, and most of the flux is absorbed in the I-front. Since the temperature increases over a larger distance, for small clouds with strong shocks a significant fraction of the cloud mass can become tied into the I-front.

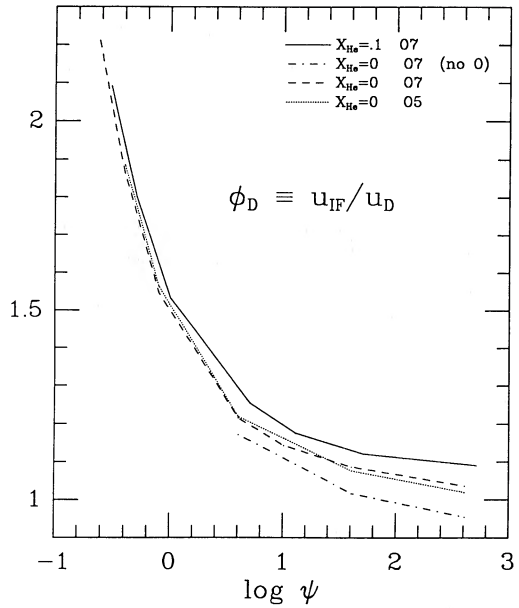

FIG. 2.—The dimensionless factor $\phi_D(\psi)$ describing the deviation of the I-front speed from the characteristic D-critical velocity u_D. The results of model calculations are plotted for 37,500 K (O7 star) and 47,000 K (O5 star, *dotted line*) blackbody ionizing radiation fields. Oxygen is included at cosmic abundance, but is left out in calculations indicated by the dash-dot line. As the front thickens significantly ($\psi < 10$), its propagation velocity increases.

2. The effective width of the region in which the incident ionizing photons are absorbed by recombining gas is ω times the radius of curvature of the I-front. The ionized boundary layer thus effectively extends out to 10%–20% of the front

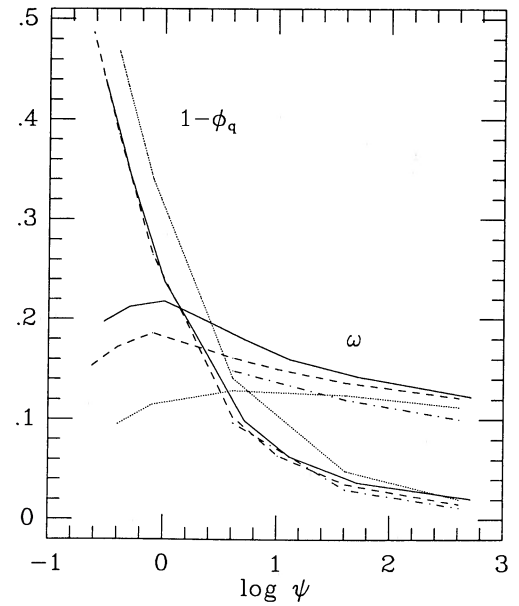

FIG. 3.—Effective width of the I-front ($1 - \phi_q$) and ionized boundary layer, ω, for different stellar temperatures and cooling metal abundances. The I-front widens significantly for small ψ.

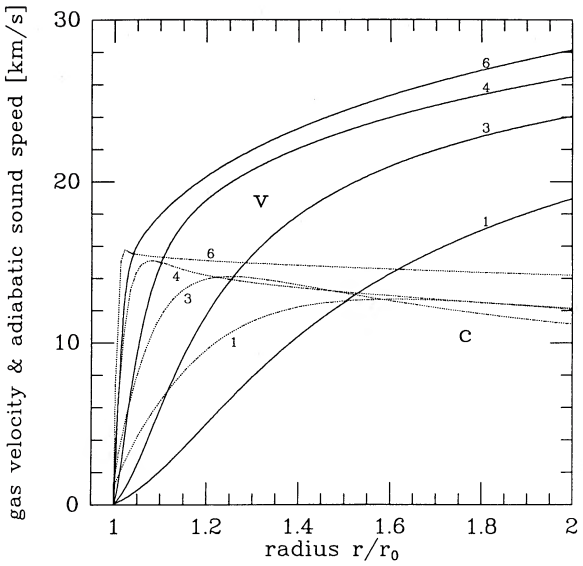

FIG. 4

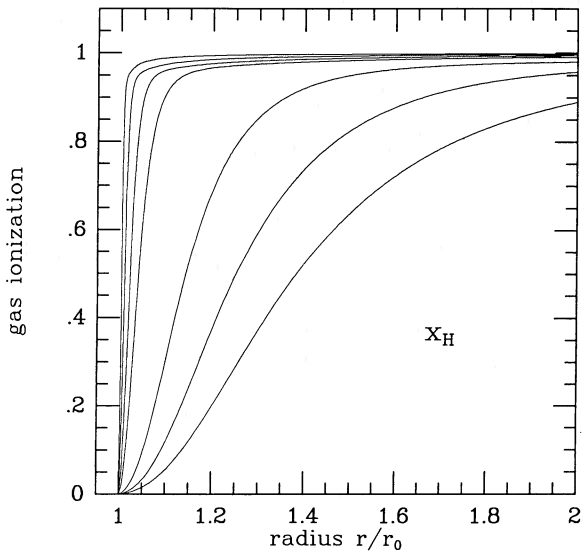

FIG. 5

FIG. 4.—Structure of spherical steady ionization fronts: the radial gas velocity (*solid curves*), v and the gas adiabatic sound speed, c (*dotted curves*), are plotted as functions of the radial distance from the neutral cloud surface for seven model calculations. With increasing velocity: models 1, 3, 4, and 6 (Table 1). The adiabatic sonic point moves out for decreasing ψ. For the thin I-front cases, the sound speed maximum coincides with the isothermal sonic point.

FIG. 5.—Hydrogen ionization, x_H, for model calculations 1–7, where the lowest curve corresponds to the model with the lowest ψ, model 1.

curvature but absorbs a significant fraction of the incident ionizing flux only for $\psi > 10$.

3. The inclusion of helium ($X_{He} = 0.1$) does not influence the overall structure of the I-front significantly. The helium I-front is always wider than the hydrogen I-front.

4. Eliminating the metal cooling does widen the I-front but does not prevent the gas from becoming supersonic, in contrast to the situation for planar fronts. The hydrogen cooling as well as the adiabatic cooling due to the spherical expansion of the gas enables the gas to cross the sonic point even if a maximum in the sound speed does not exist. Remember that in the case of a planar I-front (Kahn 1969) the isothermal sonic point is the point of maximum sound speed.

5. The color temperature of the ionizing radiation field does change the structure of the evaporation flow but does not change the velocity of the I-front (Fig. 2). We have used two blackbody ionizing spectra of color temperatures 37,500 and 47,000 K, corresponding to an O7 and an O5 star, respectively. The I-front widens for the harder spectrum, and the effective width of the IBL decreases (Fig. 3). We conclude that at least in the range we investigated, conditions at the I-front are of strong D-type and approximately D-critical, almost independent of the temperature of the ionizing spectrum. The rise in ϕ_D for low ψ is due in part to the decreasing maximum sound speed in the flow. This is due to the increasing importance of the adiabatic expansion cooling in a flow which is severely out of thermal equilibrium.

IV. EVOLUTION OF AN IONIZATION-SHOCK FRONT

In the previous section we derived the detailed structure of steady spherical ionization fronts, fronts for which the ionizing radiation field is incident parallel to the streaming motion of the ionized gas, perpendicular to the surface of the neutral cloud. The I-front was assumed to move into the cloud at a velocity small compared with the sound speed in the ionized gas. Those calculations were one dimensional and do not strictly apply to the two-dimensional flow structure off an initially spherical cloud subjected to a planar ionizing radiation field. In this section we will apply the spherical I-front structures to derive an approximate flow pattern off an axisymmetric I-front. Our treatment will have to be approximate, since an accurate solution seems beyond the bounds of an analytical treatment and requires detailed numerical computations like those we will present in Paper III.

a) Ionizing Surface Flux

Our aim is to determine the ionized gas flow structure of an axisymmetric (convex) I-front. This will yield the mass loss of

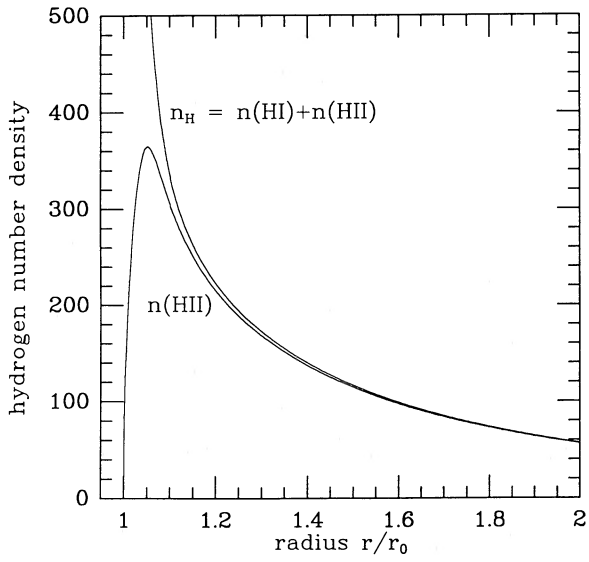

FIG. 6.—Total hydrogen number density n_H and the electron or ionized gas density, n(H II), as a function of radius from the neutral cloud for model 4.

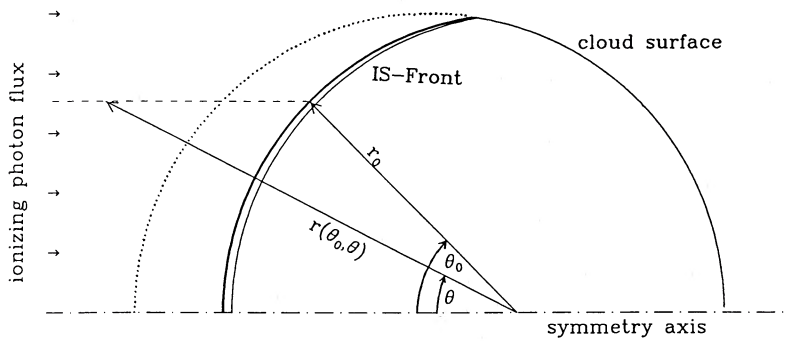

FIG. 7.—An ionization-shock front propagates into an initially spherical cloud. The ionizing photon flux at (r_0, θ_0) depends on the absorption along the (*dashed*) line toward the ionizing star.

the cloud and the momentum deposited into the shocked neutral gas. We shall make the simplifying assumption that at any point the gas flows along straight trajectories normal to the cloud surface (which is well justified in the layer where most of the ionizing photons are absorbed; Dyson 1973); the mass and momentum flux at the symmetry axis is then given by the spherical model described in the previous section. To determine the material flux off any surface point not on the symmetry axis, we would have to integrate an equation similar to equation (3.9) from that particular point to the ionizing star. We can do this for the simplified case where the I-front is spherical and very thin compared with the cloud curvature (large ψ), so that $\phi_q \simeq 1$. The result for the other extreme case, where ψ is small and all the ionizing radiation reaches the I-front, is simple: the ionizing flux per surface area reaching the front varies as the cosine of the angle between the surface normal and the direction to the star.

The total ionizing flux reaching the I-front at some angle θ_0 (Fig. 7) is equal to the incident flux, F_i, diminished by the number of recombinations to excited levels of H in a column of unit cross section extending from the ionizing source to the point on the surface under consideration. The latter is specified by the radius of curvature of the front and the azimuthal angle from the axis: (r_0, θ_0). The ionizing flux reaching the I-front at θ_0 is then

$$\phi_q F_{II}(\theta_0) = F_i - \int \alpha_{BH} n_e^2 \, ds \,, \tag{4.1}$$

where the integration is carried out along the line connecting (r_0, θ_0) with the ionizing star. The factor ϕ_q is evaluated at the symmetry axis to comply with equation (3.9).

In Appendix B we show that the *Ansatz*

$$F_{II}(\theta) = F_{II}(0) \cos^{\beta} \theta \tag{4.2}$$

yields a sufficiently accurate estimate for the angle dependence of the ionizing flux reaching the I-front. Expanding the integral in equation (4.1) for small angles θ recovers relation (3.9) and yields a value for β from -0.5 for $\psi \gg 1$ to 0 for $\psi \ll 1$, approximating expression (B5):

$$\beta \simeq -\left(2 + \frac{1.53}{q - \phi_q}\right)^{-1} . \tag{4.3}$$

Even though the *Ansatz* (4.2) should be less accurate at larger angles, we shall use it as a working formula for the subsequent discussion.

b) Propagation of the IS-Front

In order to determine the velocity and mass of the neutral gas after the IS-front has crossed the initial cloud, we would have to solve for the absorption of ionizing photons in the ionized gas streaming off the I-front simultaneously with the dynamics of the shocked gas. The IS-front dynamics determines the evolution of the surface shape of the I-front, which in turn determines the structure of the ionized flow off the I-front. Since an accurate analytic solution of this fully two-dimensional problem is out of the question, we shall make certain simplifying assumptions to obtain an estimate for the total mass loss and the final velocity of the neutral cloud after the IS-front has crossed.

To estimate the ionizing flux that reaches the I-front, we shall assume that the flow of absorbing gas reaches its steady state profile (which is strictly valid only for small shock velocities) defined by the incident ionizing flux and the curvature of the front. The ionizing flux reaching a surface element which is inclined at some angle θ to the plane of the radiation field will be described by the simple cosine power derived in the previous section. The IS-front is assumed thin and at a velocity which is determined by the pressure exerted by the I-front at a given instant. Since the IS-front loses its sphericity, we shall use the mean curvature of a given surface element. We can then propagate the IS-front from its initial location (displaced by $2r_0 \delta$ into the initial cloud, if the I-front started out R-type) up to the time when all the initial cloud gas has been swept up by the shock.

At a given time $t^* \equiv tc_i/r_0$ the surface is described by its radial and axial coordinates $y^* \equiv y/r_0$ and $z^* \equiv z/r_0$. The ionizing flux reaching the surface at a given point is approximated by the flux at a surface element with the same inclination on a tangent sphere with the same mean curvature as this point on the I-front. With $z' \equiv dz/dy = \tan\theta$ being the inclination of the front at a given surface point and time, this point's two principal curvatures are

$$K_a = \frac{d}{dy^*} \sin\theta = \frac{z''}{(1 + z'^2)^{3/2}} ,$$
$$K_b = \frac{\sin\theta}{y^*} = \frac{z'}{y^*(1 + z'^2)^{1/2}} , \tag{4.4}$$

and the tangent sphere with the same initial flow divergence has the radius $r_i^* = 2/(K_a + K_b)$. The shock velocity at this point is then approximately

$$v_s^*(y^*, t^*) = \min\left\{1, v\left[\frac{(\cos\theta)^{\beta+1}}{\phi_D q}\right]^{1/2}\right\} , \tag{4.5}$$

where q is given by $q(q - \phi_q) = \omega\psi r_i^*$ and the fudge factors are fitted (as functions of ψr_i^*) to the numerical results obtained in § III. For the reasons outlined in § II*b*(iii), the shock velocity, v_s^*, shall at all times be limited to values smaller than unity.

We have numerically propagated the IS-front for a given ψ by means of an implicit finite-difference scheme. The radial axis has been divided into 100 equally spaced grid points, each of which was propagated in axial direction with constant time steps according to

$$\frac{dz^*}{dt^*} = \frac{v_s^*}{\cos\theta},$$

where v_s^* is given by equation (4.5). Spatial derivatives are computed to second order, whereas the time propagation is implicit and first-order accurate. The cloud is completely specified by either v and η or, more conveniently, ψ and $\delta' \equiv v^2/4\eta$. In Figure 8 we compare the IS-front evolution for several exemplifying choices for these parameters. The location of those clouds is marked in Figure 1. We have also integrated the mass loss off the I-front while propagating the IS-front into the cloud. The total mass loss is plotted in Figure 9 as a function of δ' and constant ψ for the cases computed. The mass loss is compared with a simple analytic estimate we derive in § IV*c*. The turnover of the mass loss at $\delta' \simeq 1$ is due to the limiting of the IS-velocity to c_i, and the following upward bend toward unity mass loss represents the mass loss due to the initial IBL. We estimate the final cloud velocity away from the star as the integrated axial momentum of the neutral gas which is swept up by the shock, divided by the initial neutral cloud mass (excluding the initial IBL). We find that this velocity is (within 10%) 0.45 times the initial shock velocity at the symmetry axis, $v_s(\theta = 0)$, as given by equation (4.5). For clouds where $\delta \simeq 1$, the velocity of the imploded cloud tends to increase toward $v_s(0)$, but the uncertainty introduced in neglecting the dynamical effect of the initially rapidly ionized gas may be large.

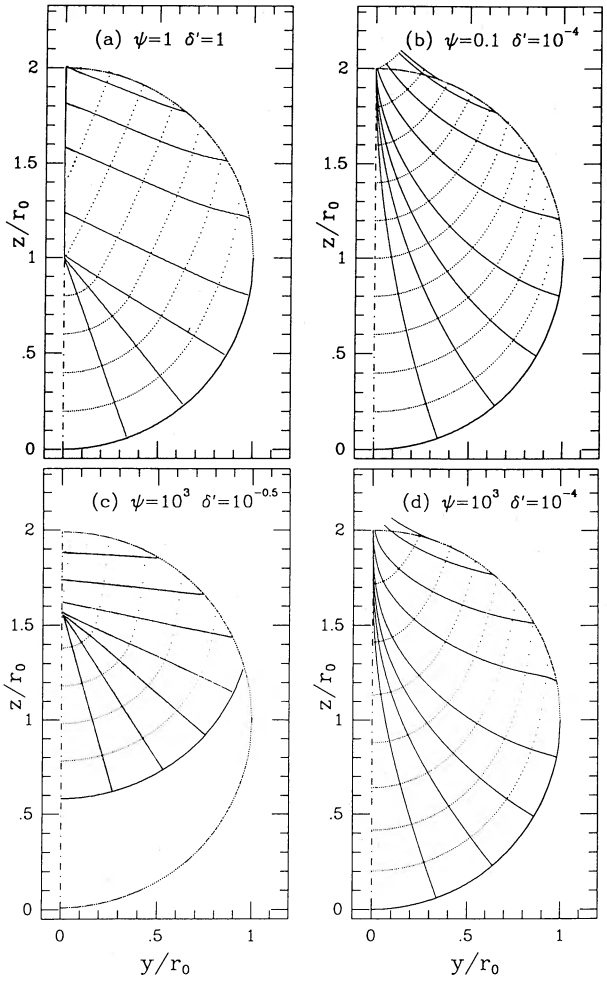

FIG. 8.—A massless, thin IS-front propagates into a spherical cloud. The location of the IS-front is indicated at equal time intervals (*dotted lines*) for four characteristic cases indicated by squares in Fig. 1. Gas particles swept up by the front propagate along the solid curved lines (which in this case are always perpendicular to the front) toward the symmetry axis, where an accretion shock should form in the second half of the compression. Including the gas inertia would steepen the trajectories of the gas approaching the axis, particularly in case (*d*). In case (*c*), an initially R-type I-front has ionized a fraction of the cloud before a shock developed, and the limiting of the shock velocity to c_i leads to an almost spherical implosion.

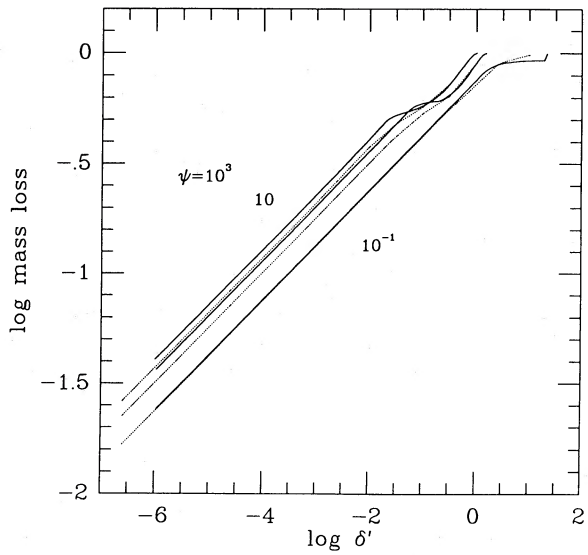

FIG. 9.—Total cloud mass loss during the radiation-driven implosion. Results from a simpleminded model calculation (eq. [4.7]) are displayed (*solid lines*) for ψ = 1000, 10, and 0.1. They are compared with the mass loss determined by the numerical integration of the IS-front propagation (*dotted lines*) as described in § IV*b*.

Note that we neglected the dynamical effect of the inertia of the gas which is swept up in the IS-front. Thus our approach will yield accurate results only when the total mass swept up in the IS-front is small compared with the initial cloud mass. If the gas inertia is neglected, the direction of motion of the neutral shocked gas is always directed normal to the IS-front surface. We can therefore trace the trajectories of gas particles which are swept up by the IS-front, and Figure 8 shows those for eight different starting points. The lines show the direction of motion of the shocked gas before it is evaporated off the I-front. In the high mass loss case, gas propagates on these lines only for a short distance, since it is evaporated off shortly after it has been shocked. In the case where a significant fraction of the cloud mass has been piled up in the IS-front, gas

which is swept up in outer regions will have to be reaccelerated in axial direction while it moves toward the symmetry axis. This will result in a less focused evolution of the IS-front. The trajectories of the gas will, on the other hand, be steeper than in the high mass loss case, since the inertia of the gas will maintain the radial momentum; the gas collides at the symmetry axis soon after the IS-front has reached the center of the initial cloud. The results of our calculation become more accurate for high-inertia IS-fronts, for which the gas trajectories are almost straight, as for the cloud shown in Figure 8*c*.

The radial velocity of the gas which collides at the axis will increase in time as gas which originated farther away from the symmetry axis, and has therefore been accelerated to higher radial velocities, reaches the axis. The gas which is evaporated off the I-front does originate predominantly in the outer regions of the cloud. When the radial velocity of the gas which collides at the symmetry axis becomes larger than its sound speed, a cylindrical accretion shock will form. We shall refer to the mass which has been accumulated inside this accretion shock as the postimplosion cloud (PIC). The size of the PIC will depend on the ram pressure of the gas accreting onto it, as well as the pressure in the PIC. The latter has three components: the thermal pressure of the gas, a turbulent pressure which will depend largely on how well the flow is collimated onto the PIC, and the pressure of the magnetic field that has been dragged into the PIC. In § V we will estimate the size of and pressure in the PIC after the IS-front has crossed the initial cloud.

c) Cloud Mass Loss

To supplement the discussion in the previous section, a simple analytic estimate for the cloud mass loss can be derived without following the exact evolution of the I-front surface.

As before, the initial cloud is assumed spherical and homogeneous. After the initial IBL has been evaporated off (for clouds with $\delta > 0$) and a steady flow of ionized gas off the I-front has been established, the IS-front will propagate into the cloud at a velocity which is given by the flux of ionizing photons reaching the I-front. For a hemispherical I-front, we have shown that the flux of ionizing photons reaching the I-front at azimuthal angle $\theta = \cos^{-1}\mu$ varies approximately as μ^{β}, where β is given by equation (B5) or equation (4.3). The I-front pressure drives a shock into the neutral cloud with a velocity $v_s(\mu) \simeq \min(c_i, v_0\,\mu^{(\beta+1)/2})$, where $v_0 \equiv v_s(\theta = 0)$ is given by equation (4.5). If the IS-front is thin (which is the case for a radiating shock and a small magnetic field component perpendicular to the propagation of the shock), then the surface of the I-front will tend to assume a more parabolic shape with a decreasing radius of curvature at the symmetry axis. We shall now simply assume that at a given distance from the symmetry axis the shock velocity and the mass flux from the I-front are constant over the shock crossing time of the cloud. The mass evaporated off the I-front at some angle θ per surface area and time is equal $u_{\rm IF}\,\rho_{\rm I}(\mu) = \phi_D\,\rho_0\,v_s^2(\mu)/2c_i$. If we divide the initial cloud into concentric cylindrical shells of mass $dm_c^* = 3\mu(\mu - \delta)d\mu$, the mass loss off the exposed side of the shell is $2\pi r_0^2\,\rho_0\,\phi_D\,v_s^2(\mu)d\mu/2c_i$ per unit time. The shock crosses the length of the cylinder in a time $2r_0(\mu - \delta)/v_s(\mu)$, and the total mass lost off the face of the shell is therefore estimated as

$$dm_i^* = \tfrac{3}{2}\phi_D\,\mu(\mu - \delta)\,\min(1, v_0^*\,\mu^{(1+\beta)/2})d\mu\,. \tag{4.6}$$

Integrating over all cylindrical shells yields the total mass lost during the clouds' compression. To obtain the total mass loss of the initial cloud, we need to add the mass of the initial IBL. With $\mu_c \equiv \max(\delta, v_0^{*\,-2/(1+\beta)})$ we then get for the total mass loss

$$\begin{aligned}\frac{m_0 - m'}{m_0} &= \int_0^1 dm_i^*(\mu) \\ &= \phi_D\left\{m_s^* + \frac{1}{2}(1 - \mu_c^3) - \frac{3}{4}\,\delta(1 - \mu_c^2)\right. \\ &\quad + \frac{3v_0^*}{7 + \beta}\left[\mu_c^{(7+\beta)/2} - \delta^{(7+\beta)/2}\right] \\ &\quad \left. - \frac{3\delta v_0^*}{5 + \beta}\left[\mu_c^{(5+\beta)/2} - \delta^{(5+\beta)/2}\right]\right\},\end{aligned} \tag{4.7}$$

where m' is the remaining neutral mass after the IS-front has crossed the initial cloud, and $m_s^* = \delta(3 - \delta^2)/2$ is the mass lost as the layer initially ionized by an R-type I-front. Figure 9 shows the total cloud mass loss according to equation (4.7) as a function of δ' for three different values of ψ and compares the results with the numerical calculations described in § IV*b*. Considering the simplicity of our approach, the results agree surprisingly well, indicating that they might not be very sensitive to the simplifying assumptions made.

d) Velocity and Mass Loss for Large ψ

For a cloud with a large photoevaporation parameter ($\psi \gg 10$), we can find simple approximate expressions for the shock velocity at the symmetry axis and the mass loss of the cloud during the radiation-driven implosion phase. For large ψ, an initial cloud gets zapped instantly when $\delta' > 1$ (cf. eq. [2.8]); a cloud of given initial density and radius is ionized without forming an ionization-shock front if its distance to the ionizing star is smaller than the zapping radius

$$R_{z,\,\rm pc} = 0.229\left(\frac{S_{49}}{n_{0,3}^2\,r_{0,\,\rm pc}}\right)^{1/2}. \tag{4.8}$$

As long as $R_0 > R_z$, an IS-front will compress the cloud, and only a fraction of the cloud mass is lost during its compression. The velocity of the IS-front at the symmetry axis is given by equation (2.5), but limited to a maximum of $v_s = c_i$, as pointed out earlier. For large photoevaporation parameter, the shock velocity is conveniently expressed in terms of the zapping radius,

$$v_s^* = \min\left[1, \left(\frac{7.8R_z}{R_0}\right)^{1/2}\right], \tag{4.9}$$

where we have assumed $\omega \simeq 0.13$ and $\phi_D \simeq 1$. Using the result from § IV*b*, the velocity of the cloud after its implosion is approximately

$$v' \simeq 0.45v_s\,, \tag{4.10}$$

and the mass loss during the radiation-driven implosion becomes

$$\frac{m_0 - m'}{m_0} \simeq \frac{v_s^*}{2}\,, \tag{4.11}$$

which is equivalent to equation (4.7) in the limiting case $\psi \gg 10$.

e) Initial Cloud Irregularities

We have shown that a strong IS-front propagating into an initially spherical and homogeneous cloud will accrete mass onto the symmetry axis, thereby forming a highly compressed and probably elongated neutral condensation. Unfortunately, in reality the initial cloud will probably display a more irregular structure than the perfect homogeneous sphere we have assumed as an initial condition. If the initial cloud has an irregular shape such that the surface of the I-front defines several distinct centres of curvature and the ionized flow off each component does not interfere with its neighbor in the regime where most of the incident photons are absorbed, then the individual components will be imploded independently, fragmenting the cloud. If the initial cloud is only slightly aspherical on the side facing the star, the shock focusing described earlier will be less pronounced and the final condensation will be less compact (as indicated by the numerical results in Sandford, Whitaker, and Klein 1982). A quantitative estimate of the mass loss and the final velocity will have to use the mean curvature of the cloud on the side facing the star, i.e., the average curvature of the I-front.

The initial cloud can also be elongated along the symmetry axis. In this case the IS-front will keep propagating into the cloud in the same way as for the spherical case, but for a longer time. The relative mass loss will be the same if it is computed using the curvature of the I-front, not the average cloud radius. The same is true for the velocity of the final condensation. The latter will probably be more elongated if the initial cloud is.

Small dents or filaments attached to the initial cloud will, because of their larger curvature, even out, evaporate off, or implode individually, and not affect the overall evolution of the cloud.

A density inhomogeneity within the initial cloud can fragment the cloud if its column density along the symmetry axis is comparable to the average cloud column density. In this case the IS-front will wrap around the clump and implode it separately from the rest of the cloud. Whenever the IS-front encounters a clump with column density smaller than the column density of the shocked gas in the IS-front, the IS-front will sweep it up without being significantly affected.

V. THE POSTIMPLOSION CLOUD

While the IS-front propagates into the cloud, a fraction of the initial cloud mass is evaporated off the I-front. The remaining mass is first piled up in the layer between the shock and ionization fronts and while the IS-front crosses the cloud eventually accretes onto the symmetry axis, forming a highly compressed globule (the PIC). Shocked neutral gas will accrete onto the PIC until the IS-front has completely crossed the initial cloud. Our approximate determination of the gas trajectories shows that most of the gas has accreted onto the PIC at the time the IS-front leaves the initial cloud volume. The difference between the phase velocity of the IS-front and the axial velocity of the PIC pointed out earlier will tend to separate the PIC from the IS-front, i.e., the IS-front will wrap around the PIC by the time the shock reaches the back of the cloud. This is a development we were not able to take into account in determining the evolution of the IS-front, but which we will address in the numerical simulations described in Paper III.

Ignoring the possibly complex interplay between the IS-front and the PIC toward the end of the compression, we will in this chapter estimate the pressure inside the PIC when it leaves the location of the initial cloud. The initial cloud shall be permeated by a uniform magnetic field, parts of which will be dragged into the PIC, where it can dominate the pressure and determine the shape of the PIC.

a) Magnetic Flux

In this section we will derive an approximate expression for the magnetic flux trapped in the postcompression cloud for a fixed initial field orientation.

In order to determine the magnetic flux which penetrates the PIC, we have to determine the original locations in the initial cloud of given gas elements in the PIC. Since the ambipolar diffusion time of the shocked gas is typically much larger than the IS-front crossing time, we can assume that the field lines are frozen to the gas, i.e., the gas can only slide along the field lines. Then the flux that crossed the volume defined by the original location of the PIC gas is equal to the magnetic flux crossing the PIC.

As long as the compression of the gas swept up by the IS-front is large, the velocity of the IS-front does not depend significantly on the initial magnetic field strength or orientation. A strong initial magnetic field will therefore not influence the gas trajectories computed in § IV*b* as long as the Alfvénic Mach number of the shock is large.

We can roughly derive the volume that the gas which ends up in the PIC has occupied in the initial cloud by examining the gas trajectories displayed in Figure 8. It is necessary to determine where, for a given trajectory, the gas particle was swept up that is evaporated exactly when it reaches the axis. Then all the particles swept up on this trajectory after that one will not be lost and will contribute both mass and the field to which they are connected to the PIC. We have done several such calculations for different cloud mass-loss rates and have concluded that this volume is approximately spherical. The magnetic flux through this volume will be dragged into the PIC. If we know the mass of the PIC relative to the initial cloud mass, m^*, then the flux through the PIC is $m^{*2/3}$ times the flux through the initial cloud. The flux-to-mass ratio increases for the PIC by $m^{*-1/3}$. If we define $\Phi^* \equiv \Phi/\Phi_0$ as the PIC magnetic flux relative to the initial cloud flux, then $\Phi^* \simeq m^{*2/3}$ is a reasonably accurate expression that we shall use in the subsequent discussion.

b) Accretion Flow

A simple estimate will yield the average accretion ram pressure that the flow of shocked gas onto the symmetry axis exerts on the PIC. Toward the end of the cloud implosion, the PIC is supported by its thermal, turbulent, and magnetic pressure, and extends a distance z^* in axial and y^* in radial direction. It contains the mass m' and is bounded by a coaxial accretion shock. In the course of the implosion, the IS-front gas accretes onto this shock with the mean radial velocity $v_y \simeq v_0/2$. Thus the mass m' accretes onto the accretion shock of area $2\pi yz$ with an average velocity v_y in a time $\simeq r_0/v_0$, and the average accretion ram pressure is of order

$$p_{ac} \simeq \frac{v_0}{r_0}\frac{m'v_y}{2\pi yz} = \rho_0 v_0^2 \frac{m^*}{3y^*z^*} . \tag{5.1}$$

c) Postimplosion Cloud without Magnetic Field

In the absence of a magnetic field, the pressure of the accreting gas is balanced by the thermal and turbulent pressure in the PIC. If the PIC pressure can be described by $c_p^2\rho_p$, where ρ_p

is the average gas density in the PIC and c_p an effective isothermal sound speed, the shock jump condition at the accretion shock, with an accretion velocity of $0.5v_0$ and the density of the accreting gas upstream given by $\rho = \rho_0(v_0/c_0)^2$, yields the pressure in the PIC as approximately

$$p_p^* \equiv \frac{p_p}{\rho_0 c_0^2} \simeq 0.25M^4 = 0.25\left(\frac{v_0}{c_0}\right)^4 . \quad (5.2)$$

The fourth-power dependence of the compression on the Mach number of colliding shocks was first derived and numerically verified by Sandford, Whitaker, and Klein (1982). With the mean density in the PIC being $m'/(\pi y^2 z)$, pressure balance at the accretion shock,

$$p_{ac} \simeq c_p^2 \frac{m'}{\pi y^2 z} , \quad (5.3)$$

yields the radial extent of the PIC as

$$y^* = 4\left(\frac{c_p}{c_0}\right)^2 M^{-2} , \quad (5.4)$$

and the axial length of the PIC becomes

$$z^* = \left(\frac{c_p}{c_0}\right)^2 \frac{m^*}{3} . \quad (5.5)$$

The axial extent of the PIC cannot exceed a distance given by the maximum widening of the IS-front due to thermal expansion in the crossing time of the cloud. Thus the shock can only widen to $2c_0 r_0/v_0$, and z^* in (5.5) has to be limited to a maximum of $2/M$. In case z^* reaches this limit, the pressure in the PIC exceeds the value given by (5.2) and is

$$p_p^* = \left(\frac{c_0}{c_p}\right)^2 \frac{m^*}{24} M^5 . \quad (5.6)$$

The radial extent of the PIC is not affected by this limitation. Let us emphasize again that we have assumed that the IS-front propagates into the initial cloud at a velocity which is large compared with the sound speed therein, so that the shocked layer of gas between the ionization front and the shock front is thin compared with the cloud radius.

The expression for the pressure of the PIC, equation (5.2), can be generalized for a gas of general adiabatic index γ. With c_0 as the isothermal sound speed in the initial cloud, and M the isothermal Mach number of the IS-front, equation (5.2) becomes

$$p_p^* \equiv \frac{p_p}{\rho_0 c_0^2} \simeq 0.25M^{2+2/\gamma} \quad (5.7)$$

d) Axial Magnetic Field

We will estimate the pressure in the PIC in the case where a uniform magnetic field permeates the initial cloud and dominates its pressure. Two limiting cases will be discussed, for which the orientation of the initial field is parallel and perpendicular to the symmetry axis. In the former case, we can estimate the dimension of the PIC as well.

Again we will consider the PIC at the time when the IS-front has almost reached the back side of the initial cloud, while mass still accretes onto the accretion shock bounding the PIC. The mass inside the accretion shock (which is assumed close to the symmetry axis) is m^*, and the magnetic flux trapped in this

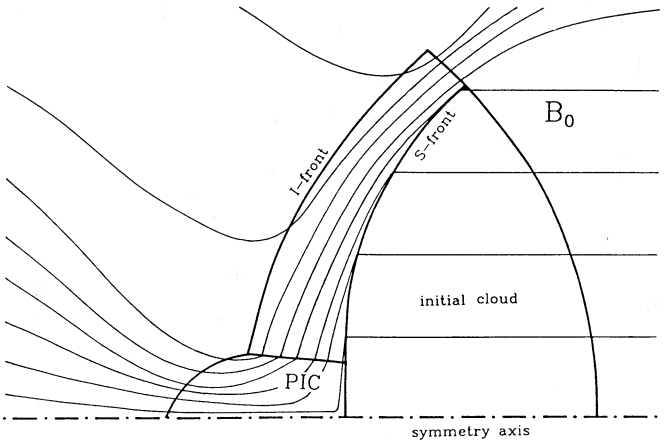

FIG. 10.—Schematic diagram of the magnetic field line configuration for an initially parallel field orientation. Most of the cloud flux enters the growing postimplosion cloud (PIC) through the IS-front. The radiation is incident from the left.

mass is $\Phi^* \simeq m^{*2/3}$. We define $M_A \equiv v_0/v_A$ and $M \equiv v_0/c_0$ as the Alfvénic and isothermal Mach numbers of the IS-front, where $v_A \equiv B_0/(4\pi\rho_0)^{1/2}$ is the Alfvénic velocity in the initial cloud.

If y is the radius of the accretion shock and z its axial extent, which is equal to the width of the IS-front at y, then the magnetic field enters the PIC through the cylindrical shock of area $2\pi yz$, and exits through an area πy^2 at the side of the PIC bounded by the I-front (Fig. 10). Just outside the accretion shock (upstream), the thickness of the IS-front is determined by the pressure of the I-front and the magnetic flux in the shocked gas accreting onto the PIC, which yields an equation for the product y^*z^*:

$$\rho_0 v_0^2 = \frac{1}{8\pi}\left(\frac{\Phi'}{2\pi yz}\right)^2 \Rightarrow y^*z^* = 2^{-1.5}\Phi^* M_A^{-1} . \quad (5.8)$$

At the accretion shock, the ram pressure of the gas streaming toward the axis has to be balanced by the pressure of the magnetic field in the PIC. All the field lines entering through the accretion shock eventually leave parallel to the symmetry axis. Thus the second jump condition,

$$p_{ac} = \frac{1}{8\pi}\left(\frac{\Phi}{\pi y^2}\right)^2 , \quad (5.9)$$

together with the equations (5.8) and (5.1), determines the pressure in the PIC,

$$p_p^* \equiv \frac{p_p}{B_0^2/8\pi} = 1.89m^{*1/3}M_A^3 , \quad (5.10)$$

as well as the radius and width of the PIC,

$$y^* = 0.85m^{*1/4}M_A^{-3/4}, \quad z^* = 0.41m^{*5/12}M_A^{-1/4} . \quad (5.11)$$

Comparing the thermal pressure in the PIC to the pressure of the I-front (ρ_p being the average density, T the temperature in the PIC),

$$\frac{\rho_0 v_0^2}{\rho_p kT/\mu_H} = 0.93\frac{b^2}{T_2} M_A^{1/4} m^{*-1/12} = O(1) , \quad (5.12)$$

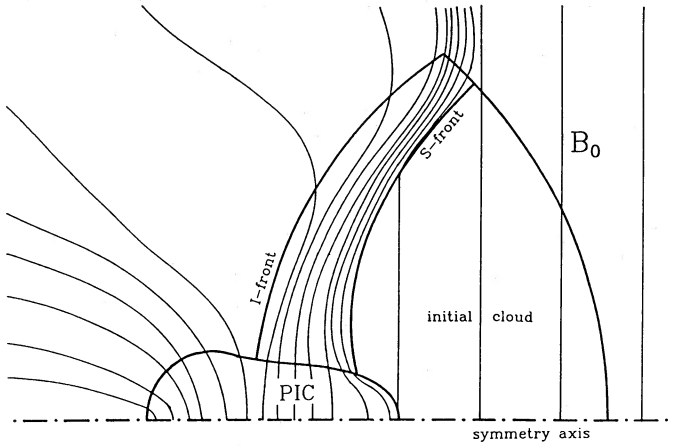

FIG. 11.—Configuration of magnetic field lines for an initially perpendicular field orientation. The cut is parallel to the initial field.

shows that the I-front can usually remain smooth at the axis, since the I-front compresses the PIC parallel to the magnetic field lines, thereby countering only the thermal gas pressure.

The argument that limited the axial extent of the PIC in the nonmagnetic case does not apply here. Since the shocked gas can expand at a velocity of the order of the Alfvén speed in the shocked gas, and the latter increases proportionally to the compression (i.e., the Alfvénic Mach number), the shock can widen sufficiently to permit an increase in IS-front width required for z^* as given in equation (5.11).

e) Perpendicular Field

The situation is more complicated when the initial magnetic field is oriented perpendicular to the line connecting the cloud with the star, and the following estimate for the pressure in the PIC is extremely crude. Even though the motion of the shocked gas can still be assumed axially symmetric, the configuration of the magnetic field becomes fully three-dimensional. Figure 11 shows the likely structure of the magnetic field just before the IS-front reaches the back of the cloud. Again, the total mass piled up within the accretion shock is m^*, and the total magnetic flux penetrating this mass is $\Phi^* \simeq m^{*2/3}$. In contrast to the parallel field case, only a fraction ε_ϕ of that magnetic flux crosses the accretion shock at that time. The accretion shock is probably not axisymmetric any more.

Consider the gas which accretes onto the axis perpendicular to the field. If z is the width of the accretion shock (and therefore the IS-front) at a radius y from the axis perpendicular to the field, balancing the accretion ram pressure with the average magnetic pressure in the part of the PIC embraced by the accretion shock (analogous to eq. [5.9]), we find

$$p_{ac} = \rho_0 v_0^2 \frac{m^*}{3y^*z^*} = \frac{B_p^2}{8\pi}, \tag{5.13}$$

with p_{ac} given by equation (5.1). Although the width of the IS-front might be larger perpendicular to this point on the accretion shock, the relation

$$\varepsilon_\phi \Phi \simeq 2yzB_p \tag{5.14}$$

will roughly describe the average field strength, B_p, in the PIC. Combining these two equations yields B_p, and thereby the average magnetic pressure in the PIC:

$$p_B^* \simeq 0.18\varepsilon_\phi^{-2} M_A^4 m^{*2/3}. \tag{5.15}$$

Judging from the calculated gas trajectories, by the time the IS-front reaches the back side of the cloud, we estimate ε_ϕ as approximately 0.5. The pressure in the PIC is larger for the perpendicular field in cases where a fraction of the flux and mass of the PIC has been squeezed out of the volume confined by the accretion shock. Since the mass not subjected to the accretion flow can expand freely, the mean pressure in the PIC is expected to be lower than that given by equation (5.15). We conclude that the PIC will probably show an inhomogeneous structure, where parts of it expand freely while others are strongly pressurized by the radial accretion flow. The mean pressure in the PIC is probably closer to the value given by equation (5.10).

VI. DISCUSSION

Photoevaporating clouds are readily observable, and it should be possible to recognize a cloud in the implosion stage and distinguish it from clouds which have settled into an equilibrium configuration (Paper II) or whose dynamics are determined by other factors like the passing of a supernova shock or a stellar wind.

In this section, we shall derive formulae that can be applied to observable clouds in H II regions. As concrete examples, we shall assume two clouds of initial density 10^3 cm^{-3}, an initial magnetic field of 30 μG, and masses of 1 and 10 $M_\odot$ at a distance of 10 pc from the central cluster of O stars ($S_{49} = 11$) in the Rosette Nebula NGC 2237−44 (see, e.g., Herbig 1974; Schneps, Ho, and Barrett 1980). These clouds may represent the initial clumps in the molecular cloud in which the Rosette Nebula was born. Many compact neutral globules are seen in the northwest quadrant of the nebula against the diffuse H II emission. The smaller globules have teardrop shapes directed toward the cluster of O stars and are isolated from the wall of molecular gas which seems to confine the nebula. Larger, more irregularly shaped (elephant trunk) clumps are seemingly tearing off the molecular shell. It seems that these clumps reflect the imploding clumps of the surrounding molecular cloud which were suddenly exposed to the ionizing radiation as the H II region expanded beyond their position. Schneps, Ho, and Barrett (1980) estimated the masses of some of the larger globules as between 1 and 10 $M_\odot$. With these masses and the assumed initial density, the initial clump radius was $r_{0,pc} = 0.20(0.42)$ for $m_0 = 1(10)\, M_\odot$. With

$$\psi = 5.15 \times 10^4 \frac{S_{49} r_{0,pc}}{R_{0,pc}^2}, \tag{6.1}$$

this yields $\psi = 1130(2380)$, and with $q(q - \phi_q) = \omega\psi$ and the factors ϕ_q and ω taken (or extrapolated) from Figures 2 and 3, we find the IBL absorption factor $q \simeq 12(18)$. Approximately one can set $q = 1$ for $\psi < 10$ and $q = (0.1\psi)^{1/2}$ for $\psi > 10$ or use the fit (10% accuracy for $0.3 < \psi < 10^3$)

$$q \simeq \tfrac{1}{8}[1 + (1 + 1.5\psi^{1/4})^2]. \tag{6.2}$$

We can further estimate the emission measure of the cloud's bright rim, the IBL. If $\psi \gg 10$, then almost all of the incident ionizing radiation is absorbed in the IBL. Then the emission measure is approximately equal to the incident flux divided by the recombination rate coefficient in the rim, and

$$\mathrm{EM} \simeq 10^5 S_{49} R_{0,pc}^{-2} \text{ pc cm}^{-6}, \tag{6.3a}$$

and for our particular case, EM = 1.2×10^4. In general, though,

$$\mathrm{EM} \simeq 2.2 \frac{\omega\psi^2}{q^2 r_{0,\mathrm{pc}}} \mathrm{pc\ cm^{-6}} = 2.2 \frac{q - \phi_q}{q} \frac{\psi}{r_{0,\mathrm{pc}}} \mathrm{pc\ cm^{-6}}, \quad (6.3b)$$

so that unless $r_0 \ll 1$ pc, the cloud must have a large value of ψ to be readily visible. The emission measure is computed along the line connecting the cloud center with the ionizing star, but the observable EM is larger if the cloud is viewed from the side. If the line of sight is perpendicular to and intersecting the line connecting the cloud and the star, the maximum emission measure is approximately a factor $2(1 + 2/\omega)^{1/2} \simeq 8$ larger than the value given by equation (6.3b).

Another observable parameter is the cloud column density or visual extinction. Many of the clouds studied by Pottasch (1956) are probably in the course of their initial implosion. The observed size of those clouds is usually indicative of their initial size, and a measurement of the column density distribution should indicate their initial column and mass density, approximately placing the observed cloud on the phase diagram (Fig. 1). The observed clouds, provided they are in their implosion stage, should never fall into region I or IV. For our two example clouds in the Rosette Nebula, $\eta = 10^{2.15}(10^{2.47})$ and $v = 10^{0.60}$ or the ionization parameter Γ is equal to $10^{-3.51}$. The clouds therefore fall into region III (stars in Fig. 1); the shocks propagating into the clouds move at velocities of $v_s \simeq 11$ km s^{-1} and the clumps gain a velocity of ~ 5 km s^{-1} away from the ionizing stars in the course of their implosion.

We can estimate the time a cloud spends in its implosion stage. The IS-front crossing time is roughly $t_{\mathrm{sc}} \sim 2r_0/v_0$, or

$$t_{\mathrm{sc}} \simeq 2.9 \times 10^5 \left(\frac{\phi_D q}{\psi}\right)^{1/2} \left(\frac{m}{M_\odot}\right)^{1/2} \mathrm{yr}, \quad (6.4)$$

which for $\psi > 10$ is given approximately by

$$t_{\mathrm{sc}} \simeq 2 \times 10^5 \psi^{-1/4} \left(\frac{m}{M_\odot}\right)^{1/2} \mathrm{yr}, \quad (6.5)$$

and for $\psi < 10$ is

$$t_{\mathrm{sc}} \simeq 3 \times 10^5 \psi^{-1/2} \left(\frac{m}{M_\odot}\right)^{1/2} \mathrm{yr}. \quad (6.6)$$

Clouds with high emission measure have either large ψ or small masses (corresponding to small r_0), hence usually have crossing times smaller than the main-sequence lifetime $t_{\mathrm{ms}} \simeq 4.4 \times 10^6 S_{49}^{-1/4}$ yr (McKee, Van Buren, and Lazareff 1984) of an O star. For the two example clouds we find shock crossing times of 3.4×10^4 (8.8×10^4) yr, which is short compared with the lifetime of the most luminous (O4) star in the cluster, as well as compared with the dynamical age of the H II region derived from the observed velocities of the H II and molecular gas (Schneps, Ho, and Barrett 1980) of (4–7) $\times 10^5$ yr.

While a clump is in its implosion stage, its neutral gas is distributed very unevenly. Higher density gas should be concentrated in the layer of shocked gas preceding the I-front, and a clump of high pressure and density forms at the symmetry axis at later times during the implosion. For magnetically dominated clouds, the density of the gas in the IS-front depends on the Alfvénic Mach number of the penetrating shock. Clouds are magnetically dominated if the Alfvén velocity in the initial cloud exceeds its thermal sound speed. If we can relate the initial cloud magnetic field to its density by $B_0 = 10^{-6} b n_0^{1/2}$, then the Alfvén speed is $v_{\mathrm{A}} = 1.84b$ km s^{-1}, which is for $b \simeq 1$ typically larger than the cloud thermal sound speed. In § V*d* we derive the pressure we expect in the PIC. From equation (5.10), the magnetic field strength in the PIC is found as

$$B \simeq 635 \left(\frac{n_{0,3}}{b}\right)^{1/2} v_s^{*3/2}\ \mu\mathrm{G}, \quad (6.7)$$

where the shock velocity $v_s^* \equiv v_s/c_i = v/(\phi_D q)^{1/2}$ and $v^2 = 2\psi/\eta$. We can compare this with the initial cloud field of $B_0 = 32 b n_{0,3}^{1/2}\ \mu$G. Note that the large field in the PIC is observable only during the final phase of the compression. After this, the PIC can expand and the field strength decreases again.

As a very different application of our theory, we can investigate the fate of intergalactic neutral clouds (Lyα clouds) when they are first exposed to the ionizing radiation of a single QSO. Donahue and Shull (1987) have pointed out that those clouds typically get ionized without ever developing an IBL. If the total ionizing flux from the QSO is $S = 10^{56} S_{56}$ s^{-1} and a cloud with a neutral column density $N_{\mathrm{H}} = 10^{17} N_{\mathrm{H},17}$ cm^{-2} and number density $n_0 = 10^{-3} n_{-3}$ cm^{-3} is placed at a distance $R = 10^6 R_{\mathrm{Mpc}}$ pc from the QSO, we can compute $\Gamma = 10^{-1.55} S_{56} R_{\mathrm{Mpc}}^{-2} n_{-3}^{-1}$ and $\eta = 10^{-1.62} N_{17}$. Typical intergalactic clouds therefore clearly fall into region IV of Figure 1, i.e., they get "zapped" by an R-type I-front and never develop a shock or an IBL. A zapped cloud, which may initially have been in pressure equilibrium with the intergalactic medium, will expand and dissipate unless it again reaches a pressure equilibrium with the intercloud medium. A cloud does not get zapped and a shock will form and compress the neutral gas when

$$\delta = \frac{1540 S_{56} R_{\mathrm{Mpc}}^{-2} n_{-3}^{-1} - 4}{0.095 N_{17}} \simeq 1.6 \times 10^4 \frac{S_{56}}{R_{\mathrm{Mpc}}^2 n_{-3} N_{17}} < 1. \quad (6.8)$$

Only then will part of the cloud remain neutral as it is imploded by the dynamical effects of the QSO's ionizing radiation.

VII. SUMMARY

In this paper we described the initial evolution of a cosmic gas cloud when it is suddenly exposed to strong ionizing radiation. Although the general conclusions are valid for any source of ionizing radiation, we have specifically studied the evolution of an interstellar cloud which is exposed to a newly formed massive star.

Generalizing the historic work of Oort and Spitzer and of Kahn, we have studied in detail the structure of spherical ionization fronts and ionized boundary layers of clouds exposed to a planar radiation field. We have done this even in cases where the recombination length in the IBL is so large that essentially none of the incident ionizing photons are absorbed therein and the ionization front cannot be considered thin compared with its radius of curvature. It was shown how the structure of an I-front depends on the cooling metal abundances, the effects of the helium ionization, and the spectral type of the ionizing star. For a wide range of parameters, the ionized gas expands supersonically into the intercloud medium, and conditions at the I-front are approximately D-critical. Usually the I-front drives a shock into the initial cloud

with a velocity of up to the sound speed in the ionized gas. The compression of the gas that has been swept up by the shock depends mostly on the strength of the magnetic field in the initial cloud.

The two main parameters which classify the initial cloud are its column density (or visual extinction) and an ionization parameter which describes the density of the ionizing radiation field relative to the cloud density. The space defined by these two parameters can be divided up into several regions which include clouds with significantly different evolutions. Clouds with small column densities or those very close to the ionizing source are instantly ionized and expand into the intercloud medium. For clouds where the penetrating ionization front slows down to develop a shock front before it reaches the back of the cloud, only part of the initial cloud mass is lost during the subsequent ionization-driven implosion. The remaining gas will get highly compressed as the IS-front focuses the neutral shocked gas onto the symmetry axis of the initial cloud. A cylindrical accretion shock forms that confines a globule in which the pressure is determined by the cloud magnetic field and the velocity of the IS-front. After all the initial cloud mass has been swept up by the IS-front, the postimplosion cloud moves away from the ionizing star at a velocity of up to half the sound speed in the ICM, which is typically 5 km s^{-1}.

Because of the large compression of the gas in the PIC, nonmagnetic clouds which were initially gravitationally stable can become supercritical and collapse to form stars. In the presence of magnetic fields, the field has to diffuse out of the compressed cloud before it can become gravitationally unstable (Bertoldi, Klein, and McKee 1990).

In Paper II we will discuss the subsequent fate of the PIC. If gravitational effects are not important, the PIC is bounded by an I-front which exerts a pressure that eventually has to balance the PIC's internal pressure. We will show that the PIC will then be able to settle into an equilibrium configuration, slowly evaporating while accelerating away from the ionizing source.

I wish to express my thanks to Chris McKee for his patient advice and support throughout the course of this work. I would also like to thank Richard Klein for helpful comments and many interesting discussions. This work was supported in part by NSF grants AST83-14684 and AST86-15177 and in part under the auspices of a special NASA Astrophysics Theory Program which supports a joint Center for Star Formation Studies at NASA–Ames Research Center, the University of California at Berkeley, and the University of California at Santa Cruz.

APPENDIX A

IONIZING RADIATION FIELD

The ionizing radiation spectrum is divided into two parts: at a given radius r, $F_1(r)$ will denote the total ionizing photon flux between 1 and 1.808 rydbergs, the ionization edge of helium. Correspondingly, $F_2(r)$ is the flux beyond the helium edge. An ionizing photon in bin 1 (1–1.808 Ry) is absorbed by a hydrogen atom with an average absorption cross section $\bar{a}_1$, creating a photoelectron with an average kinetic energy of $\bar{E}_1$ Ry. Correspondingly, the averaged absorption cross sections in bin 2 (1.808–10 Ry) are $\bar{a}_{2\mathrm{H}}$ and $\bar{a}_{2\mathrm{He}}$ and the photoelectron energies $\bar{E}_{2\mathrm{H}}$ and $\bar{E}_{2\mathrm{He}}$, for hydrogen and helium absorption, respectively. The averaged quantities in bin 1 are functions of $F_1/F_{1,i}$, and those in bin 2 are functions of both $F_1/F_{1,i}$ and $F_2/F_{2,i}$, and have been computed for a blackbody spectrum of a given stellar temperature T_*. Note that $F_{1,i} + F_{2,i} = F_i$.

The diffuse radiation due to hydrogen ground-state or helium $n = 1$ and $n = 2$ recombinations has been treated in the on-the-spot approximation, i.e., all the created photons are reabsorbed at the radius at which they were emitted.

The ionization equations for H and He are coupled by the radiation field in frequency bin 2. The photons emitted in recombinations to the ground level of He can ionize either H or He, and the fraction absorbed by H is (Osterbrock 1974)

$$\mathscr{y} = \left(1 + 6.34 X_{\mathrm{He}} \frac{1 - x_{\mathrm{He}}}{1 - x_{\mathrm{H}}}\right)^{-1}, \tag{A1}$$

while the remaining fraction, $(1 - \mathscr{y})$, is absorbed by He. Helium bound-bound transitions from $n = 2$ to $n = 1$ produce photons that can ionize H but not He. The total number of recombinations to excited levels of He per unit volume and time is $x_{\mathrm{He}} n_{\mathrm{He}} n_e \alpha_{\mathrm{BHe}}$, and of those a fraction $p \simeq 0.96$ (Osterbrock 1974) generate photons that are absorbed on the spot in the low-density limit. Thus, in the on-the-spot approximation, the ionization equations become

$$\begin{aligned} v\frac{dx_{\mathrm{H}}}{dr} &= (\bar{a}_1 F_1 + \bar{a}_{2\mathrm{H}} F_2)(1 - x_{\mathrm{H}}) - n_e[x_{\mathrm{H}} \alpha_{\mathrm{BH}} - x_{\mathrm{He}} X_{\mathrm{He}}(\mathscr{y}\alpha_{1\mathrm{He}} + p\alpha_{\mathrm{BHe}})] , \\ v\frac{dx_{\mathrm{He}}}{dr} &= \bar{a}_{2\mathrm{He}} F_2(1 - x_{\mathrm{He}}) + x_{\mathrm{He}} n_e[(1 - \mathscr{y})\alpha_{1\mathrm{He}} - \alpha_{\mathrm{AHe}}] . \end{aligned} \tag{A2}$$

The equations for the ionizing radiation flux are

$$\begin{aligned} \frac{dF_1}{dr} &= n_{\mathrm{H}} F_1 \bar{a}_1(1 - x_{\mathrm{H}}) , \\ \frac{dF_2}{dr} &= n_{\mathrm{H}} F_2[\bar{a}_{2\mathrm{H}}(1 - x_{\mathrm{H}}) + \bar{a}_{2\mathrm{He}} X_{\mathrm{He}}(1 - x_{\mathrm{He}})] . \end{aligned} \tag{A3}$$

Equations (A2) and (A3) can be combined to yield an equation for the electron abundance relative to hydrogen. With $x_e \equiv n_e/n$ and $F = F_1 + F_2$,

$$nv \frac{dx_e}{dr} = \frac{dF}{dr} - n_{\rm H} n_e [x_{\rm H} \alpha_{\rm BH} + x_{\rm He} X_{\rm He}(1-p)\alpha_{\rm BHe}] . \tag{A4}$$

APPENDIX B

IONIZING SURFACE FLUX

The ionizing photon flux reaching the I-front at some angle θ_0 (Fig. 7) is given by equation (4.1). At a given point (r, θ) in the flow, the recombination rate will be a function of both $r^* \equiv r/r_0$ and θ. With $r^* = \sin\theta_0/\sin\theta$, $n_{\rm II}(\theta) \equiv F_{\rm II}(\theta)\cos\theta/c_i$ and $ds = r\,d\theta/\sin\theta$, we can rewrite equation (4.1) as

$$\phi_q F_{\rm II}(\theta_0) = F_i - \frac{\psi}{F_i} \int_0^{\theta_0} F_{\rm II}^2(\theta) \mathscr{R}(r^*, \theta) \frac{\sin\theta_0}{\tan^2\theta} d\theta , \tag{B1}$$

where

$$\mathscr{R} \equiv \frac{\alpha_{\rm BH} n_e(r^*, \theta) n_p(r^*, \theta)}{\alpha_i n_{\rm II}^2(\theta)}$$

is a normalized recombination rate, which for spherical fronts is only weakly dependent on ψ, the parameter describing how much of the incident flux reaches the I-front (Fig. 12). To a good approximation we can assume that outside the I-front (or sonic point) $\mathscr{R}$ can be fitted by a power law with a power index ε which is independent of θ and similar to that of the § III fronts:

$$\mathscr{R}(r^*, \theta) \simeq \mathscr{R}(r^*, 0) \equiv \omega(\varepsilon - 1) r^{*-\varepsilon} . \tag{B2}$$

Again, ω, as defined in equation (3.11), is determined at $\theta = 0$. This approximation is justified because the flux reaching the I-front at different θ will not vary too much over most of the surface, a condition that has to be confirmed when an estimate for $F_{\rm II}(\theta)$ is found.

Making the *Ansatz* $F_{\rm II}(\theta) \propto \cos^\beta\theta$ for the θ dependence of the ionizing flux reaching the I-front, and substituting equation (B2) in equation (B1), yields

$$q(q - \phi_q \cos^\beta\theta_0) = \psi\omega(\varepsilon - 1)(\sin\theta_0)^{1-\varepsilon} \int_0^{\theta_0} (\cos\theta)^{2\beta+2} (\sin\theta)^{\varepsilon-2} d\theta . \tag{B3}$$

We can expand the terms in this equation for small values of θ, integrate, and compare the zero- and second-order terms (the first order vanishes), which yield

$$q(q - \phi_q) = \psi\omega \tag{B4}$$

and

$$\beta = -\left[2 + \frac{\varepsilon + 1}{(q - \phi_q)(\varepsilon - 1)}\right]^{-1} , \tag{B5}$$

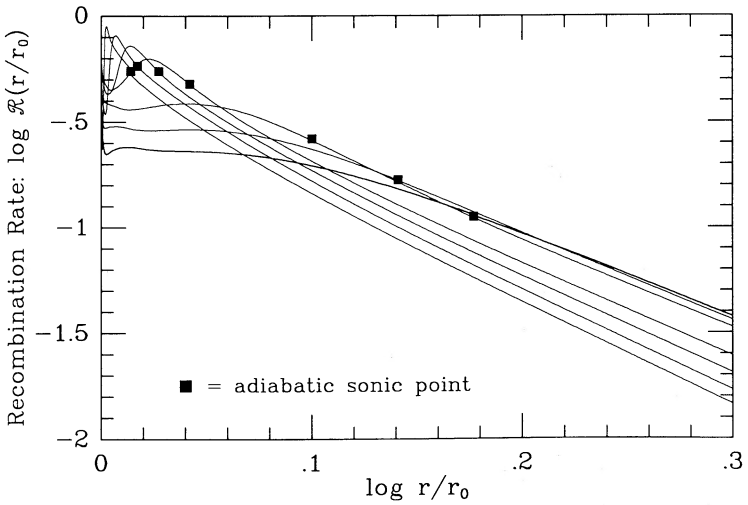

FIG. 12.—Normalized recombination rate as defined in eq. (B1) for model calculations 1–7 (Table 1) can be described by a power law outside the sonic point. The power index is only weakly dependent on ψ.

respectively. We find that β ranges between $-\frac{1}{2}$ (for large ψ and q) and 0 (for $q \simeq \phi_q$). To show how insensitive β is to the slight change in the functional dependence of $\mathscr{R}$ on r^* for changing q, we use the results of our model calculations from § III. These show that outside the sonic point, $\mathscr{R}(r^*)$ is approximated by a power law of index $\varepsilon = 5$ for $q \simeq 10$ or 4.5 for $q \simeq 1$. Thus $(\varepsilon + 1)/(\varepsilon - 1)$ becomes 1.5 and 1.57, respectively, a change of less than 10% for a change in q by an order of magnitude. This justifies the approximation made in equation (B2). We could have fitted the normalized recombination rate $\mathscr{R}$ by a power series with more than one term, but this would not have altered this conclusion, and would have only an insignificant effect on the numerical value of β.

With equation (B5), we find that $F_{\rm II}(\theta_0)\cos\theta_0$, the ionizing flux per surface area reaching the I-front at θ_0, will have dropped by an order of magnitude at $\theta_0 > 85°$. Thus, over most of the surface, with the insensitivity of β to the incident flux, the assumption of one β determined at $\theta = 0$ is reasonably accurate. Of course we have assumed that the flow off the I-front is similar to the one-dimensional flow we have investigated in § III. A more accurate treatment would have to take into account that the ionizing radiation is incident at an oblique angle for $\theta > 0$. Therefore, our *Ansatz* becomes more inaccurate for large angles, but we shall adopt it as a working formula for the subsequent discussion.

APPENDIX C

GLOSSARY OF SYMBOLS

a_{jX}	Photon absorption cross section in frequency bin j (1 or 2) for element X
$\bar{a}$	Frequency-averaged hydrogen absorption cross section
$\bar{A}_V$	Initial cloud visual extinction
c	Adiabatic sound speed ($\gamma = 5/3$)
c_0	Initial cloud isothermal sound speed
$c_{\rm I}$	Isothermal sound speed in the shocked cloud gas
c_i	Isothermal sound speed in the ionized ICM at 10^4 K
C	Speed of light
$\bar{E}_{jX}$	Average photoelectron excess energy from H/He ionization in frequency bin $j = 1,2$
F_i	Ionizing (Lyman continuum) photon flux at cloud location
$F_{\rm II}$	Lyman continuum flux reaching the I-front
F_j	Ionizing photon flux in frequency bin $j = 1, 2$
k	Boltzmann constant
$K_{a,b}$	Principal curvatures on axisymmetric surface
l_a	Absorption length at the I-front
M	Isothermal Mach number of the IS-front $\equiv v_s/c_0$
$M_{\rm A}$	Alfvénic Mach number of IS-front at the symmetry axis
m_0	Initial cloud mass
m'	Cloud mass after implosion
n_i	Number density of gas nuclei in the ionized ICM
n_0	Number density of gas nuclei in the initial cloud
$n_{\rm H}$	Hydrogen number density
$n_{\rm He}$	Helium number density
n_e	Electron number density
$n_{\rm I}$	Density of neutral shocked gas nuclei
$n_{\rm II}$	Typical ionized gas density at the I-front
p	Fraction of He excited level recombination photons reabsorbed by H
$p_{\rm ac}$	Ram pressure of gas accreting onto PIC
p_p	Pressure in PIC
p_B	Magnetic pressure in PIC
q	Ratio between incident ionizing flux and gas flux leaving the cloud at the symmetry axis
r_0	Initial cloud radius
R_0	Initial cloud-star separation
S	Star's photon emission rate beyond the Lyman limit
$t_{\rm sc}$	Initial cloud shock crossing time
T_i	Characteristic temperature in the ionized gas
T_0	Initial cloud temperature
$u_{\rm IF}$	Velocity of the I-front relative to the shocked neutral gas
u_D	D-critical I-front velocity
v	Gas velocity relative to the I-front
$v_{\rm A}$	Alfvén velocity
v_s	Velocity of the IS-front
v'	Velocity of the PIC
x_e	Gas ionization
$x_{\rm H}$	H ionization

x_{He}	He ionization
X_{He}	Ratio of He to H number density
y	Radial distance from symmetry axis
$\mathscr{Y}$	Fraction of He ground-state recombination photons reabsorbed by H relative to He
z	Axial coordinate
α_{BH}	H electronic recombination coefficient to excited states
α_{BHe}	He electronic recombination coefficient to excited states
α_{AHe}	He electronic recombination coefficient to all states
α_{1He}	He electronic recombination coefficient to ground state
α_i	α_{BH} at characteristic temperature 10^4 K
β	Power of cos θ dependence of ionizing flux reaching the I-front
Γ	Ionization parameter
Γ_h	Gas heating rate
δ	Width of initial ionized boundary layer
δ'	Width of initial Strömgren layer $\equiv v^2/4\eta$
δ_{gr}	Standard extinction deviation factor
ε_ϕ	Fraction of magnetic flux through PIC crossing accretion shock
η	Dimensionless initial cloud column density
Λ	Gas cooling rate
μ_H	Gas mass per hydrogen nucleus
v	Velocity parameter $\equiv v_s/c_i$
ρ	Gas mass density
ϕ_q	Dimensionless parameter for width of the I-front
ϕ_D	Ratio of I-front velocity to D-critical velocity
Φ	Magnetic flux threading the cloud
φ	Dimensionless velocity integration parameter
ψ	Dimensionless product of incident flux and cloud curvature: photoevaporation parameter
ω	Effective fractional thickness of the recombination layer (IBL)
IBL	Insulating ionized gas boundary layer, recombination layer
PIC	Postimplosion cloud

REFERENCES

Axford, W. I. 1961, *Phil. Trans. Roy. Soc. London, A*, **253**, 301.
Bertoldi, F., Klein, R. I., and McKee, C. F. 1990, in preparation.
Bertoldi, F., Klein, R. I., McKee, C. F., and Sanford, M. T. 1990, in preparation (Paper III).
Bertoldi, F., and McKee, C. F. 1990, *Ap. J.*, submitted (Paper II).
Blitz, L. 1987, in *Physical Processes in Interstellar Clouds*, ed. G. Morfill and M. Scholer (Dordrecht: Reidel), p. 35.
Dalgarno, A., and McCray, R. A. 1972, *Ann. Rev. Astr. Ap.*, **10**, 375.
Dibai, E. A. 1960, *Soviet Astr.—AJ*, **4**, 13.
———. 1963, *Soviet Astr.—AJ*, **7**, 606.
Donahue, M., and Shull, M. J. 1987, *Ap. J. (Letters)*, **323**, L13.
Dyson, J. E. 1968, *Ap. Space Sci.*, **1**, 388.
———. 1973, *Astr. Ap.*, **27**, 459.
Elmegreen, B. G. 1976, *Ap. J.*, **205**, 405.
Elmegreen, B. G., and Lada, C. J. 1977, *Ap. J.*, **214**, 725.
Goldsworthy, F. A. 1961, *Phil. Trans. Roy. Soc. London, A*, **253**, 277.
Herbig, G. H. 1974, *Pub. A.S.P.*, **86**, 604.
Jura, M. 1975, *Ap. J.*, **197**, 575.
Kahn, F. D. 1954, *Bull. Astr. Inst. Netherlands*, **12**, 187.
———. 1958, *Rev. Mod. Phys.*, **30**, 1058.
———. 1969, *Physica*, **41**, 172.
Klein, R. I., Sandford, M. T., II, and Whitaker, R. W. 1980, *Space Sci. Rev.*, **27**, 275.
Klein, R. I., Whitaker, R. W., and Sandford, M. T., II. 1985, in *Protostars and Planets II*, ed. D. Black and M. Matthews (Tucson: University of Arizona Press), p. 340.
Leung, C. M. 1985, in *Protostars and Planets II*, ed. D. Black and M. Matthews (Tucson: University of Arizona Press), p. 104.
McKee, C. F., Van Buren, D., and Lazareff, B. 1984, *Ap. J. (Letters)*, **278**, L115.
Melia, F. 1988, *J. Comput. Phys.*, **74**, 488.
Mendis, D. A. 1969, *M.N.R.A.S.*, **142**, 441.
Oort, J. H., and Spitzer, L. 1955, *Ap. J.*, **121**, 6.
Osterbrock, D. E. 1974, *Astrophysics of Gaseous Nebulae* (San Francisco: Freeman).
Pérault, M., Falgarone, E., and Puget, J. L. 1985, *Astr. Ap.*, **152**, 371.
Pottasch, S. R. 1956, *Bull. Astr. Inst. Netherlands*, **13**, 77.
———. 1958*a*, *Bull. Astr. Inst. Netherlands*, **14**, 29.
———. 1958*b*, *Rev. Mod. Phys.*, **30**, 1053.
Reipurth, B. 1983, *Astr. Ap.*, **117**, 183.
Sanford, M. T., Whitaker, R. W., and Klein, R. I. 1982, *Ap. J.*, **260**, 183.
Schneps, M. H., Ho, P. T. P., and Barrett, A. H. 1980, *Ap. J.*, **240**, 84.
Shu, F. H., Adams, F. C., and Lizano, S. 1987, *Ann. Rev. Astr. Ap.*, **25**, 23.
Shull, P., Jr., Dyson, J. E., Kahn, F. D., and West, K. A. 1985, *M.N.R.A.S.*, **212**, 799.
Spitzer, L. 1968, in *Stars and Stellar Systems*, Vol. **7**, *Nebulae and Interstellar Matter*, ed. B. M. Middlehurst and L. H. Aller (Chicago: University of Chicago Press), p. 1.
———. 1978, *Physical Processes in the Interstellar Medium* (New York: Wiley).
Tielens, A. G. G. M., and Hollenbach, D. 1985, *Ap. J.*, **291**, 722.

FRANK BERTOLDI: Princeton University Observatory, Peyton Hall, Princeton, NJ 08544